Refining the Evolution of Gas-Particle Partitioning in Cooking Emissions Oxidation via FIGAERO-CIMS Analysis

Ruizhe Shen[1], Song Guo[1,2]*, Hui Wang[1], Ying Yu[1], Zichao Wan[1], Rui Tan[1], Wenfei Zhu[1], Zheng Chen[1], Shiyi Chen[1], Zhijun Wu[1], Shuangde Li[3], Yunfa Chen[3], Min Hu[1,2]

[1]State Key Laboratory of Regional Environment and Sustainability, International Joint Research Center for Atmospheric Research (IJRC), College of Environmental Sciences and Engineering, Peking University, Beijing, 100871, China
[2]Collaborative Innovation Center of Atmospheric Environment and Equipment Technology, Nanjing University of Information Science & Technology, Nanjing, 210044, China
[3]State Key Laboratory of Multiphase Complex Systems, Institute of Process Engineering, Chinese Academy of Sciences, Beijing, 100190, China

Correspondence to: Song Guo (songguo@pku.edu.cn)

Abstract. Cooking emissions are increasingly important sources of organic aerosol in densely populated urban areas as controls reduce emissions from industrial and fossil-fuel combustion. Their atmospheric evolution and environmental and health effects remain difficult to assess because of the complexity of their composition and transformation pathways. Here, we conducted a laboratory study of emissions from heated corn oil using a Go:PAM oxidation flow reactor. We investigated the evolution of composition, volatility, and gas-particle partitioning and evaluated discrepancies between FIGAERO-based measurements and thermodynamic estimates. FIGAERO-I-CIMS measurements combined with a 2-D VBS parameterization were used to characterize the composition and volatility distributions of primary and secondary cooking aerosol. Kinetic calculations indicate that particle-phase diffusion is unlikely to be the dominant resistance under the modeled conditions and that the major components of the secondary organic aerosol are at or near gas-particle partitioning equilibrium. Gas-phase transport in the low-number-concentration primary aerosol and surface desorption of a limited high-molecular-weight fraction may contribute to kinetic deviations. The thermodynamic comparison nevertheless reveals a substantial unresolved gap between FIGAERO-derived volatility and equilibrium estimates, reflecting combined measurement and model uncertainties. These results clarify the scope of kinetic limitations in cooking-aerosol oxidation and identify priorities for improving the representation of cooking emissions in atmospheric studies.

1 Introduction

Secondary organic aerosols (SOA) constitute a major component of submicron atmospheric particles on both global and regional scales. (Hallquist et al., 2009) Anthropogenic SOA, particularly prominent in densely populated regions, originate from and exert considerable impacts on human society(Guo et al., 2020). While emissions from industrial and transportation sectors have been increasingly regulated under clean-air initiatives, cooking emissions—associated with specific lifestyles—are emerging as significant sources of atmospheric volatile organic compounds (VOCs), semi-/intermediate-volatility organic

compounds (S/IVOCs), and SOA precursors. Moreover, cooking represents a persistent source of indoor emissions in households, catering facilities, and restaurants, and accounting for over 20% of indoor activity time. Notably, indoor SOA formation may pose greater health risks than outdoor SOA in urban settings, given the substantial amount of time people spend indoors. Additionally, cooking emissions exhibit high spatial heterogeneity across urban areas, with emission profiles and environmental impacts varying considerably by regional culinary practices, leading to substantial uncertainties in emission estimates(Zhu et al., 2021). Therefore, effective clean-air policies aimed at mitigating cooking emissions require precise quantification of both emission characteristics and atmospheric transformation pathways.

Current research on cooking emissions has primarily focused on quantifying primary gaseous and aerosol components, along with variations linked to culinary practices. Key influencing factors encompass dish type (e.g., Eastern vs. Western cuisines, domestic cooking styles), ingredient profiles (food and oil varieties), and cooking conditions (oil temperature, seasoning usage, etc.). The gas phase is dominated by short-chain carbonyls and aliphatic acids, whereas the particle phase is rich in long-chain aliphatic acids. Other weakly oxygenated species derived from thermal decomposition and ingredient–oil interactions—such as sterols and polycyclic aromatic hydrocarbons (PAHs)—also contribute significantly to aerosol composition(Lin et al., 2021). These emissions demonstrate strong SOA formation potential in urban, suburban, and even indoor environments. (Zeng et al., 2020; Guo et al., 2023) However, the gas-particle partitioning of organic compounds during the transformation of cooking emissions remains poorly understood, primarily due to the complexity and dynamic evolution of organic composition throughout emission and aging processes. This knowledge gap represents a major challenge in atmospheric chemistry. Since gas-particle partitioning directly influences the environmental and health impacts of both primary and secondary organic aerosols, understanding on detailed mechanism within evolution processes of organic aerosols is essential for accurate risk assessment and effective air quality management.

Unlike standardized industrial or transportation emissions, primary and secondary composition characteristics of cooking emissions varies among distinct influence factors including cooking style, cooking materials (e.g. oil type, food type) and spice addition.(Rogge et al., 1991; He et al., 2004; Zhao et al., 2007; Li et al., 2015). High variety of primary organic species and complex secondary transformation process led to diverse emission and evolution characteristics(Zeng et al., 2020; Zhu et al., 2021; Tan et al., 2023; Lu et al., 2024). While most techniques rely on chromatographic separation to achieve high chemical resolution, thus temporal resolution remains limited (Song et al., 2023; Yang et al., 2023), this study integrates non-targeted analysis with high-resolution chemical ionization time-of-flight mass spectrometry (HR-ToF-CIMS) coupled to a Filter Inlet for Gases and Aerosols (FIGAERO). By employing matrix factorization and ordinal analysis, we aim to resolve the compositional features and gas–particle dynamics of cooking aerosols during oxidation, thereby elucidating the quantitative and compositional evolution of cooking-derived SOA under atmospheric conditions. Moreover, current studies focusing on thermodynamic and kinetics of gas-particle partitioning themes in cooking aerosols mainly focus on compositional characteristics of primary emissions or bulk properties of secondary cooking aerosols, molecular-resolved gas-particle partitioning thermodynamics and kinetics of secondary aerosols are limited to a certain extent(Takhar et al., 2019; Takhar et

al., 2021; Masoud et al., 2022; Kristensen et al., 2023; Sun et al., 2026) . This study will give a comprehensive insight into gas-particle partitioning thermodynamics and kinetics based on PMF deconvolution and thermodynamic estimation theories.

2 Material and methods

2.1 Experimental setup

Oxidation experiments of cooking emissions are conducted in a domestic lifestyle emission laboratory utilizing a Go:PAM Oxidation flow reactor (OFR) (Wang et al., 2021). Detailed experimental setup has been presented in previous work (Yu et al., 2022). Briefly, Go:PAM reactor operates under mode OFR254, which OH radical are generated from reaction between $O(^1D)$ radicals and water vapor. OFR254 represent atmospheric oxidation processes dominated by OH radical at low-medium NO_x concentration(Peng and Jimenez, 2020). OH exposure in the Go:PAM system is controlled by varying ozone concentration, relative humidity, and the experimental sample gas flow rate through the Go:PAM reactor. OH exposure is estimated using semi-empirical parametrizations in OFR254 recommended by Peng et al., based on measured OH reactivity, ozone concentration and relative humidity (Peng et al., 2016). Cooking experiments were conducted in a custom-made fry pan directly connect to pure nitrogen as carrier gas to avoid interference of high NO_x in ambient air on radical oxidation and I-CIMS detection. Cooking emissions are generated by heating corn oil to 120~130 °C, representing the evolution of widely used cooking oil during typical domestic cooking activities, and to certain extent representing frying and stir-frying activities widely used in both Eastern and Western cooking types(Rogge et al., 1991; He et al., 2004; Abdullahi et al., 2013; Bandowe et al., 2021).For reproducibility, we performed 4 times. It should be noted that this experiment represents a controlled, low-NOx oil-heating case rather than the full range of cooking emissions, thus the results should not be directly extrapolated to NOx-rich cooking plumes. The use of an OFR can introduce OH suppression, altered RO2 chemistry, secondary photolysis, and enhanced fragmentation; therefore, the OH-exposure-to-atmospheric-age conversion is used only as an approximate reference. Detailed experimental conditions and setup are presented in **Section S1, Supplement Information 1**.

2.2 Instrumentation

Instrumentations in this study consist of three categories, including oxidation condition, aerosol size and mass distribution of aerosols, and chemical composition of gas. For oxidation conditions in the Go:PAM reactor, ozone concentration are monitored using Thermo® model 49i ozone analyzer. Organic species in the gas phase, including precursors and low-molecular-weight oxidation products, are quantified on-line using Vocus-PTR instruments. Aerosol size distribution before and after entering Go:PAM is measured by two Scanning Mobility Particle Sizer (SMPS) systems. SPMS before Go:PAM consists of TSI® model 3080 DMA & model 3776 CPC and SMPS after Go:PAM model 3082 DMA & model 3772 CPC. Particle density measurement adopted Cambustion® Centrifugal Particle Mass Analyzer (CPMA) for total mass estimation at various OH exposure level(Zhao et al., 2007; Zhang et al., 2020; Abdullahi et al., 2013). Molecular composition, gas-particle partitioning,

and volatility of organic aerosols and are determined by a FIGAERO inlet coupled to HR-ToF-CIMS instrumentation developed by Aerodyne Inc® that choose iodide as reagent ion. Operation of FIGAERO-CIMS instrument in laboratory oxidation experiments has been since the instrumentation firstly developed (Lopez-Hilfiker et al., 2014; Le Breton et al., 2019; Bannan et al., 2019). Briefly, the FIGAERO inlet consists of a gas-phase sampling inlet that pull air directly into the API interface and IMR of CIMS instrument, and an aerosol inlet that collect aerosol samples onto a PTFE filter. One analyzes cycle is completed by a 15-min gas-phase inlet sampling period when particles collected onto the filter at aerosol inlet, a 15-min particle phase thermal desorption period when 320°C heated air for thermal desorption flush through the filter and increase filter temperature linearly from room temperature to 180°C, a 15-min continuous heating scheme for completing aerosol sample desorption, and a 15-min cooling scheme. FIGAERO inlet provides the possibility of determining both gas phase and particle phase concentration, and thus gas-particle partitioning information combined with high-resolution composition data acquired by CIMS instrumentation (Lopez-Hilfiker et al., 2016). Gas-particle partitioning coefficient K_p, defined similar to phase- equilibrium coefficients between gas-phase and particle-phase organic species, can be determined by average CIMS signal during gas-phase and aerosol phase measurements, and OA concentration determined by mass concentration instrumentations such as SMPS or AMS. Volatility of organic species can be determined separately from gas phase measurements by thermal desorption characteristics (so-called Thermograms) during linear heating process in the measurement cycle (Bannan et al., 2019). Sensitivity and volatility calibrations have been proceeded adopting certain authentication standards relevant in primary and secondary cooking emissions and following atmospheric transformations (Ylisirniö et al., 2021).Sensitivity of components without authentication standards are estimated by custom developed non-targeted analysis method. Iodide-CIMS is selective toward polar and oxygenated compounds and may underrepresent weakly oxygenated or nonpolar material. Accordingly, the molecular-composition and 2-D VBS distributions reported here describe the detectable iodide-CIMS ion ensemble rather than a mass-complete representation of all cooking emissions(Iyer et al., 2016). Trace sulfur-containing formulas were not used for mechanistic source interpretation because the corn-oil-only experiment contained no sulfur-rich food ingredients and the low-abundance signals may reflect background, contamination, or formula-assignment uncertainty(Zhang et al., 2020; Song et al., 2022). Detailed operation and data process of various instruments, sensitivity and volatility calibration methods, and quantification of species without authentication standard are presented in **Section S2, Supplement S1**.

2.3 Two-Dimensional Volatility Basis Set (2-D VBS) framework construction

The Two-Dimensional Volatility Basis Set (2-D VBS) framework has been developed to characterize the complex composition of organic aerosols in laboratory experiments, ambient observations, and modeling studies. This approach distributes organic species in 2-D gridded area with variation of mean carbon oxidation state $\overline{OS_c}$ and saturation vapor concentration C^*(Donahue et al., 2011; Donahue et al., 2012; Chuang and Donahue, 2016). Gas- and particle-phase composition and gas-particle partitioning parameters (including partitioning coefficients K_p) of primary emissions and secondary oxidation experiments are visualized in 2-D VBS space, to intuitively display the composition evolution of organic aerosol and its gas-particle partitioning

characteristics. Saturation vapor concentration in the 2-D VBS space are estimated using elemental composition from I-CIMS detection using an empirical parameterization recommended by Li et al. (Li et al., 2016). Detailed adoption of 2-D-VBS approach is shown in **Section S3, Supplement Information 1**.

2.4 Positive-Matrix-Factorization (PMF) analysis

HR-ToF-CIMS enables the detection of thousands of ions, corresponding to a comparable number of chemical species. In the present study, the FIGAERO-CIMS instrument detected 936 assignable ions corresponding to specific compounds in both gas phase and secondary organic aerosol (SOA). Complex feature of cooking aerosols and atmospheric evolution required adoption of deconvolution methods, and to extract interpretable composition and volatility patterns from the complex dataset of experimental concentration profiles, and to select representative species from species at various oxidative exposure in oxidation of cooking aerosols. In this study, we proceed various factorization and data pre-treat methods, and choose Positive Matrix Factorization (PMF) via the Igor Pro®-based SoFi® ME-2 PMF software (Canonaco et al., 2013; Buchholz et al., 2020b). In addition, ordinal analysis methods, as previously established by Kong et al. and applied in PMF factor interpretation of organic aerosols, are adopted to identify key species most abundant compounds within each resolved factor. (Kong et al., 2021). Detailed factorization method assignments are shown in **Section S4, Supplement Information 1.**

2.5 Gas-particle partitioning thermodynamics

Gas-particle partitioning thermodynamics of cooking organic aerosols are discussed comparing FIGAERO measurements and theoretical estimation. Estimated gas-particle partitioning parameters are estimated based on absorption partitioning theory and compared to FIGAERO concentration measurements(Pankow, 1994). Experimental K_p values are derived from paired FIGAERO gas- and particle-phase measurements together with the measured organic-aerosol mass concentration reported in Table S6.1. For the equilibrium calculation, the organic mass fraction is assumed to be unity, the mean particle-phase molecular weight is calculated as an concentration-weighted value for the detected organic composition. For fingerprint species extracted from CIMS detection based on PMF and ordinal analysis(Buchholz et al., 2020a; Kong et al., 2021), saturation vapor pressure are estimated utilizing SIMPOL(Pankow and Asher, 2008), and activity coefficients are calculated by AIOMFAC, and to ensure whether liquid-liquid phase separation will occur within cooking POA and SOA, , aerosol phase molar-fraction based activity are calculated (Zuend and Seinfeld, 2012) (https://aiomfac.lab.mcgill.ca/). Kelvin effect is correction is adapted assuming a typical surface tension of 0.05 $N \cdot m^{-2}$(Cai and Griffin, 2003; Schmedding et al., 2025). Gas-particle partitioning kinetics are discussed accounting for gas-phase diffusion, aerosol-phase diffusion, surface accommodation and particle coagulation. We calculate the characteristic time τ of processes in gas-particle partitioning, compared them with retention and oxidation times in the Go:PAM flow tube. Detailed gas-particle partitioning schemes are shown in **Section S5, Supplement Information 1**.

3 Results and discussion

3.1 Size & mass Distributions evolution of cooking organic aerosols in oxidation process

Figure 1 illustrates evolution of size and mass distributions from primary to secondary cooking aerosols with enhancement of OH exposure throughout oxidation experiment. Detailed size and mass distribution characteristics of aerosols are shown in **Table S6.1**, **Supplement S1.** Primary cooking aerosols exhibit a relatively broad size distribution, with particle diameters ranging from 50 to 300 nm. These particles are generally formed through physical processes such as oil evaporation, or thermal chemical reactions including oxidation and decomposition. Primary cooking aerosols comprise of components with large molecular size and relatively low carbon oxidation states, such as long-chain alkanes, alkenes, alkanals, alkenones, fatty acids and their glycerol esters, and steroids(Rogge et al., 1991; Nolte et al., 1999). In contrast, secondary organic aerosols are predominantly nanoparticles exhibiting monomodal distribution, with major aerosols diameter below 50 nm. SOA mass and size distribution exhibits rapid and substantial increase in both number and mass once exposed to OH radical as oxidant, even under the lowest OH concentration conditions, secondary aerosol number concentrations can reach up to 10^6 #·cm^{-3}. Mode diameter of SOA increased from 14.1nm to 31.1nm with enhancement of OH exposure from ~10^9 to 10^{10} #·cm^{-3}·s, while total number concentration increases from 1.37 to 3.42×10^6 #·cm^{-3}. This indicate that increasing OH exposure further enhances mass concentration predominately through particle size growth rather than number increase, implying that the dominate driving force of SOA growth is condensation rather than coagulation. Notably, particles larger than 90 nm show minimal changes in number and mass concentration, with average declination of less than 20% even under the highest OH exposure conditions (**Fig. S6.1**, **Supplement S1**). These findings collectively suggest that secondary organic aerosols from oil boiling originate mainly from nucleation and condensation of gas-phase oxidation products, rather than from oxidative aging of primary aerosols(Tan et al., 2023; Zhang et al., 2023). The observed low reactivity of primary cooking aerosols during oxidation may be attributed to the low miscibility between nonpolar or low-polarity primary components and newly formed highly polar secondary compounds (Chandramouli et al., 2003; Milsom et al., 2021; Liu et al., 2025) , likely resulting from limited partitioning tendency of primary components.

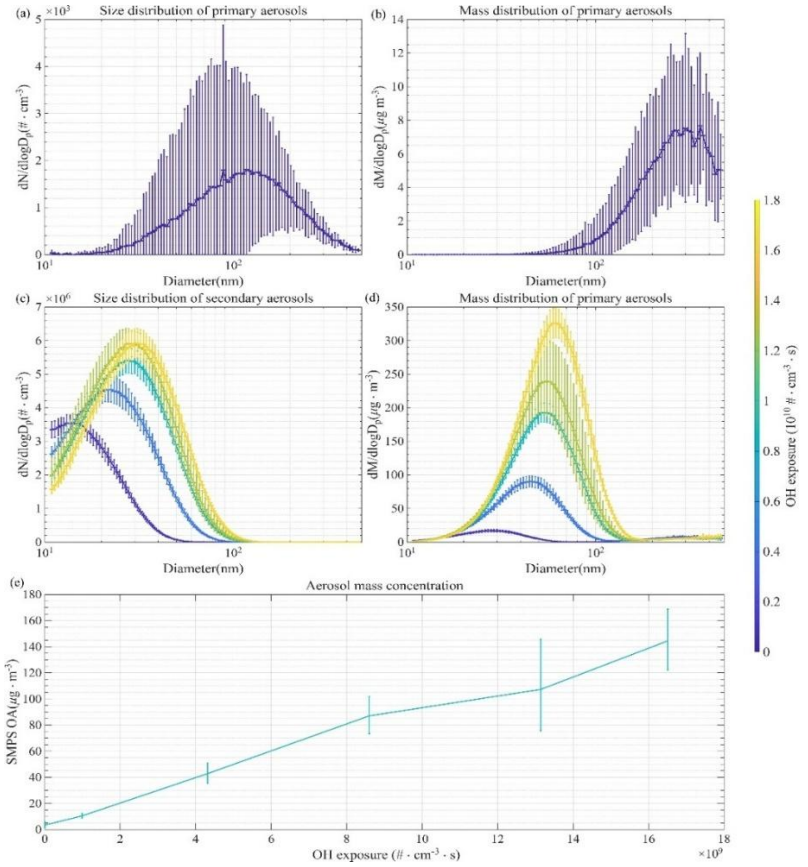

Figure 1 Primary and Secondary aerosol size & mass distribution evolution with OH exposure increases. (a) (b)illustrate size and mass distribution of primary particles, (c) (d) size and mass distribution of secondary aerosols at OH exposure 0.1~1.8×10^{10} cm^{-3} s. (e) exhibits mass concentration evolution with oxidation process from primary to OH exposure 1.8×10^{10} cm^{-3} s.

3.2 Composition and volatility distribution of primary and secondary organic aerosols in 2-D VBS Space

Figure 2 displays the volatility and compositional distribution of cooking aerosols and associated gas-phase organic components within the two-dimensional volatility basis set (2-D VBS) framework (Donahue et al., 2012). Average composition and volatility evolution are shown in **Table 1**. The majority of primary and secondary organic species are distributed in the semi-volatile and intermediate-volatile organic compound (S/IVOC) range, with an average carbon oxidation state (OSc) spanning from –1.25 to 0.5. Throughout the oxidation experiment, increasing OH exposure led to a substantial growth in S/IVOC components, consistent with the trend observed for aerosol particles. Additionally, the formation of low-volatility, highly oxidized compounds derived possibly from multi-generation oxidation is also promoted.

In gas phase, the average molecular size increases significantly during oxidation, whereas the carbon oxidation state remains nearly constant or exhibits a slight decrease following OH radical addition. This behavior may be attributed to the generation of gas-phase oxidation products via cleavage of primary long-chain fatty acids, polymerization among oxidation intermediates, and the depletion of primary low-molecular-weight organic acids resulting from glycerol thermal decomposition, such as

formic acid, acetic acid, and glyceric acid (Zhang et al., 2018; Takhar et al., 2022). By contrast, compositional shifts in the aerosol phase within the 2-D VBS space—such as in oxidation state and molecular size—are relatively minor compared to those in the gas phase. The oxidative state changes of particle-phase organics with enhanced OH exposure is relatively minor, with only marginal growth in molecular dimensions. The relatively small molecular size of primary cooking aerosols may result from the limited detection sensitivity of iodide-adduct CIMS toward nonpolar or low-polarity compounds with large molecular weights and fewer oxygen-containing functional groups, e.g., long-chain hydrocarbons, fatty acids, and steroids (Iyer et al., 2016). These compositional patterns suggest that SOA formation and growth is governed primarily by gas-phase oxidation and condensation of secondary S/IVOCs in gas phase, rather than by continuous oxidation within the particle phase. Observation implies that the oxidation process in the flow tube has approached a "steady-state turning point," particularly for particle-phase products, which reach this stage earlier owing to their oxygen-rich nature, such as $C_{>6}$ dicarboxylic acids and peroxides with carbon numbers. These products, formed through oxidation of long-chain primary acids and carbonyls, exhibit lower volatility, higher viscosity and lower oxidation rate, thereby slowing subsequent oxidative aging (Milsom et al., 2021). Detailed 2-D VBS distribution of primary and secondary organic matter in gas and aerosol phase are shown in **Supplementary Material S2**.

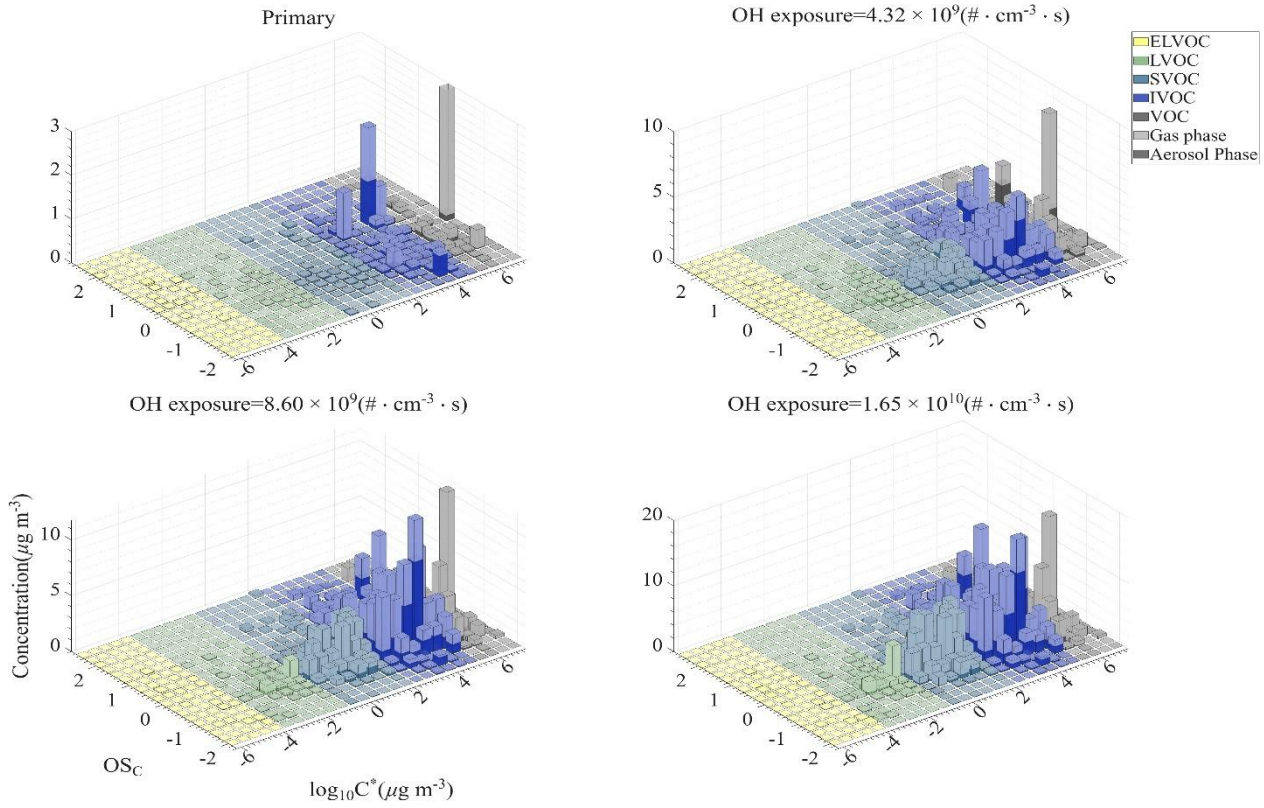

Figure 2 Distribution of gas-phase and aerosol-phase primary and secondary cooking organic species in 2-D VBS space with oxidation

Table 1 Average molecular composition and volatility parameters of primary and secondary organic components in gas phase and aerosol phase

OH exposure ($cm^{-3}\cdot s$)	Molecular composition	$\log_{10}C^0(\mu g\cdot m^{-3})$	OS_C
Primary	$C_{3.5}H_{5.4}O_{2.6}N_{0.03}S_{0.01}$*	6.0*	-0.11*
	$C_{7.1}H_{10.3}O_{3.8}N_{0.09}S_{0.03}$**	2.8**	-0.47**
4.32×10^9	$C_{5.8}H_{9.5}O_{3.7}N_{0.07}S_{0.04}$*	3.5*	-0.45*
	$C_{7.3}H_{11.9}O_{3.8}N_{0.04}S_{0.01}$**	2.8**	-0.63**
9.60×10^9	$C_{6.6}H_{10.6}O_{4.0}N_{0.07}S_{0.05}$*	2.8*	-0.49*
	$C_{7.8}H_{12.9}O_{4.0}N_{0.04}S_{0.01}$**	2.4**	-0.67**
1.65×10^{10}	$C_{7.0}H_{11.0}O_{4.2}N_{0.07}S_{0.06}$*	2.3*	-0.47*
	$C_{7.8}H_{13.0}O_{4.1}N_{0.04}S_{0.01}$**	2.2**	-0.65**

* Gas phase **Aerosol phase

3.3 Classification and Quantification of Primary and Secondary Cooking Emissions by PMF Analysis

ME-2 PMF methods are adopted in deconvolution and non-targeted analysis of FIGAERO-CIMS detections on gas-phase and aerosol-phase organic compounds with different volatility and oxidative state, so as to classify typical organic species, and extract evolution pattern corresponding to oxidation mechanism and changes of gas-particle partitioning from complex CIMS data matrix (Buchholz et al., 2020a; Hashimoto et al., 2022; Kong et al., 2021). Detailed PMF recommended factor determination methods are shown in **Section S4 of Supplement S1**. **Figure 3** shows the optimized ME-2 PMF results of FIGAERO-CIMS data. The FIGAERO-CIMS results are divided into 13 factors, including 5 pure gas-phase factors, 3 semi-volatile factors with considerable and comparable amounts both in gas phase and aerosol phase, and 4 pure aerosol-phase factors. Factors are listed in **Fig. 3** and classified by its volatility (partitioning coefficient K_p while total amount is countable) and oxidative state (mean oxidative state OS_C and evolution with enhancement of OH exposure). Detailed factor classification and interpretation procedure is shown in **Section S4 of the Supplement S1**. Formic acid (at m/z 173, detected as $ICH_2O_2^-$ in CIMS) are not included in PMF analysis due to its extreme high abundance in gas phase primary emissions and low oxidative states compared to other species (up to 25ppb, shown in **Fig. S6.3**), and would be separately discussed here. High abundant of formic acid at ppb in indoor sources and cooking emissions at ppb level has been reported in pervious researches on cooking emission (Reyes-Villegas et al., 2018; Farmer et al., 2019). Formation of cooking originated formic acid possibly due to thermal decomposition of glycerol in primary species; The relative fragile structure of glycerol-related skeleton(e.g. glycerol, lactic acid, acrylic acid, and pyruvic acid) would favor the formation of formic acid originated from thermal oxidation and decomposition, leading to high abundance of formic acid in gas-phase primary emissions (Nolte et al., 1999; Farmer et al., 2019; Zhang et al., 2021; Takhar et al., 2022; Ye et al., 2012). Primary formic acid would decline slower than estimated from OH radical reactivity (formic acid decline about 22% at OH exposure ~10^{10} $cm^3\cdot s^{-1}$) at OH exposures in current research

(Farmer et al., 2019; Atkinson et al., 2006), indicating secondary source of formic acids, possibly by ozonolysis of unsaturated compounds and further oxidation of glycerol-related species(Farmer et al., 2019; Takhar et al., 2021; Zhang et al., 2021).

Among factors, we would first classify the 13th factor as more closely to a background factor as shown in **Fig. S6.4** due to unreasonable thermogram including ill-shaped multiple distinct peaks at different desorption temperature. This factor is named Background, apart from other factors classified by volatility and oxidative states. Intensity of factor Background is relatively low, showing that contaminant would not be able to interfere measurement result too much. Among reasonable factors, V-Pri (**Figure S6.5**) and SV-Pri (**Figure S6.8**) are classified as primary emissions. The average elemental composition and most abundant species of V-Pri and SV-Pri are shown in **Table S6.2-S6.3**. Factor V-Pri stands for gas-phase primary emission, mainly consist of low-molecular-weight oxygenated organic compounds such as short chain carboxylic acids and their deviates(Masoud et al., 2022; Ye et al., 2012; Zhang et al., 2021). Most abundant compounds in Factor V-Pri are $C_{1\text{-}3}$ oxygenated organic species, such as $C_3H_4O_2I^-$ (m/z 198.93, iodide adduct, **Figure S6.6**) corresponding to acrylic acid, $C_2H_4O_2I^-$ (m/z 186.92, iodide adduct) corresponding to acetic acid, $C_3H_8O_3I^-$ (m/z 218.95, iodide adduct) corresponding to glycerol. These compounds probably originate from thermal oxidation or thermal decomposition of glycerol, which are formed by thermal decomposition of oil esters (Nawar, 1969; Nolte et al., 1999; Martins et al., 2013; Lopez-Pedrajas et al., 2018; Reyes-Villegas et al., 2018). Lesser abundant compounds in V-Pri are larger less-oxygenated compounds with carbon number >5 and oxygen number ≤2, probably formed from thermal decomposition of fat followed by thermal oxidation processes long-chain aliphatic acids, including $C_6H_{12}O_2I^-$ (m/z 242.99, iodide adduct, **Figure S6.7**) corresponding to hexanoic acid and $C_5H_{10}O_2I^-$ (m/z 228.97, iodide adduct) corresponding to pentatonic acid (Takhar et al., 2022; Takhar et al., 2021; Nolte et al., 1999; Qian et al., 2026; Xiao et al., 2023). Semi-volatile factor SV-Pri contains semi- and intermediate- volatile organic compounds with medium carbon number (5 carbons on average) and higher oxidative state than V-Pri. Most abundant compounds are $C_{3\text{-}6}$ and $O_{2\text{-}3}$ compounds, which may correspond to organic acid derivatives, such as hydroxy acids and carbonyl acids that originate from thermal oxidation of long-chain aliphatic acid in primary emissions. Compound detected as $C_5H_4O_4I^-$ (m/z 254.91, iodide adduct, **Figure S6.11**), possibly corresponding to furan-structure compounds such as aconic acid or hydroxy furoic acid, has the highest intensity in SV-Pri. $C_5H_4O_4$ present mostly in gas phase during primary emission, while particle-phase abundance increases with oxidation age increasing, indicating its possible primary thermal oxidation and dehydration origin, leading to gas-phase degradation and partitioning toward aerosol phase while SOA concentration significantly increases(Kawada et al., 1967; Nawar, 1969; Grebenteuch et al., 2021; Xiao et al., 2023; Yao et al., 2024; Hou et al., 2025). Other typical compounds abundant in SV-Pri with similar evolution characteristics includes long-chain aliphatic acids, such as palmitic acid ($C_{16}H_{32}O_2I^-$, m/z 383.14, iodide adduct, **Figure S6.9**), oleic acid ($C_{18}H_{34}O_2I^-$, m/z 409.16, iodide adduct, **Figure S6.10**). These typical primary organic compounds have evolution trends similar to $C_5H_4O_4$, with increasing are apparently abundant in gas phase and aerosol phase, but with lower concentration than small molecules ones, probably due to the quantification uncertainty of sensitivity estimation of lower-oxygenated long-chain organics(Lee et al., 2014; Chiaia et al., 2024; Zhou et al., 2022). Gas-particle partitioning of other typical species mostly abundant in factor SV-Pri such as $C_5H_8O_3I^-$ (m/z 254.91, iodide adduct, **Figure S6.12**) show different evolution pattern other than primary compounds, implementing two distinct origins of these

compounds: primary formation from gas-phase thermal oxidation, and secondary formation from oxidation of primary emissions(Zeng et al., 2020; Masoud et al., 2022; Yao et al., 2024).

Factors with intermediate oxidative state, including V-OxiGen^{1st}-Gly, V-OxiGen^{1st}-FA, SV-OxiGen^{1st} and LV-OxiGen^{1st}-Gly^{TD} (**Figures S6.13-16**), achieve highest abundance at medium oxidative exposure. Among these factors, V-OxiGen^{1st}-Gly and LV-OxiGen^{1st}-Gly^{TD} are factors with smaller molecular size, reach its peak concentration at lower OH exposure，while V-OxiGen^{1st}-FA and SV-OxiGen^{1st} reaches maximum at higher oxidative state and contains larger molecules. Typical volatile intermediate -oxidative-state factor V-OxiGen^{1st}-Gly mainly consist of two distinct categories of species. The first is $C_{2\text{-}3}$ oxygenated compounds that are higher-oxidized than corresponding compounds abundant in V-Pri, such as $C_3H_4O_3I^-$ (m/z 214.92, iodide adduct, possibly pyruvic acid, **Figure S6.6**) and $C_2H_4O_4I^-$ (m/z 214.92, iodide adduct, **Figure S6.17**) that may originate from first-generation OH oxidation or ozonolysis of glycerol-related compounds. The other is $C_{4\text{-}7}$ oxygenated compounds at intermediate oxidative exposure with medium oxidative state, such as $C_5H_{10}O_3I^-$ (m/z 244.97, iodide adduct, **Figure S6.18**) and $C_7H_{12}O_3I^-$ (m/z 214.92, iodide adduct, **Figure S6.20**), corresponding to first-generation scissoring product of long-chain fatty acids during OH and ozone oxidation, or ozonolysis, or first-generation thermal oxidation products(Takhar et al., 2021; Takhar et al., 2022; Liu et al., 2024). Factor LV-OxiGen^{1st}-Gly^{TD} have similar average oxidative state and molecular size with V-OxiGen^{1st}-Gly, seems corresponding to gas phase portion of first-generation oxidation products represented by V-OxiGen^{1st}-Gly. However, thermal desorption thermogram of LV-OxiGen^{1st}-Gly^{TD} peaks at ~440K, showing that compounds represented by LV-OxiGen^{1st}-Gly^{TD} have much lower volatility than molecular composition corresponding to this factor, indicating LV-OxiGen^{1st}-Gly^{TD} representing oxidation products of long-chain fatty acids that retaining their hydrocarbon chain(Frankel et al., 1983; Patrikios et al., 1994; Martins et al., 2013; Aladedunye, 2016; Bonetti and Parker, 2019; Lopez-Hilfiker et al., 2019; Zeng et al., 2020; Brown et al., 2021), which may have elemental composition of $C_{16/18}H_{30\text{-}34}O_{3\text{-}6}$. Particle-phase reactions between possible peroxides (such as $C_7H_{12}O_5$ and $C_9H_{16}O_5$ that abundant in V-OxiGen^{1st}-Gly and LV-OxiGen^{1st}-Gly^{TD}) and substituted alcohols or aldehydes ($C_6H_{12}O_3$ or $C_6H_{10}O_3$, etc.) accelerated by thermal desorption at lower oxidative stage may also be an alternative source(Luo et al., 2024; Qian et al., 2026). Volatile factor V-OxiGen^{1st}-FA and semi-volatile factor SV-OxiGen^{1st} share similar molecular composition such as overall oxidation state, molecular size and typical species. These species, mostly $C_{4\text{-}6}$ acids in gas phase and $C_{9\text{-}10}$ carbonyl acids in aerosol phase, have larger molecular size. These factors are totally generated from oxidation of fatty acids rather than compounds related to glycerol that are abundant in lower-oxidative-exposure factors. Moreover, comparing thermal desorption properties with molecular composition, species in Factor SV-OxiGen^{1st} represent compounds with exact molecular formula detected by CIMS rather than thermal decomposition products(Reyes-Villegas et al., 2018; Masoud et al., 2022; Takhar et al., 2021). Overall, Typical intermediate compounds are pyruvic acid in gas phase, $C_{5\text{-}10}$ carbonyl acids in both phase and large-molecular oxidation products $C_{16/18}H_{30\text{-}34}O_{3\text{-}4}$ in the aerosol phase.

Highly-oxygenated factors include volatile factors V-MultiGen-Gly and V-MultiGen-FA, semi-volatile factor SV-MultiGen-peroxy, low-voaltile factors LV-Multigen-HMW, LV-Multigen-COOH, LV-Multigen-peroxy (**Figures S6.26-31**). These factors reach highest intensity at highest experimental oxidative exposure. Among factors, V-MultiGen-Gly and LV-Multigen-

HMW are lesser oxidized, the amount of these factors reaches steady state while oxidative exposure increases to maximum in the experiment. Other factors are highly oxidized: their abundance increases significantly during oxidative exposure growth. Typical gas phase species are highly oxidized termination products of glycerol-related species, such as $C_3H_4O_4I^-$ (m/z 230.91, iodide adduct, probably malonic acid, **Figure S6.19**) and $C_3H_6O_4I^-$ (m/z 232.93, iodide adduct, probably glyceric acid), or low-molecular-weight fragmentation products of fatty acid oxidation, such as $C_4H_6O_4I^-$ (m/z 244.93, iodide adduct, probably succinic acid, **Figure S6.33**) and $C_6H_{10}O_4I^-$ (m/z 244.93, iodide adduct, probably adipic acid, **Figure S6.32**). These highly oxidized low-molecular weight compounds are more semi-volatile rather than volatile species(Zeng et al., 2020; Masoud et al., 2022; Takhar et al., 2021). Aerosol phase compounds are mostly $C_{7\text{-}10}H_{12\text{-}16}O_{4\text{-}6}$ compounds that may corresponding to $C_{7\text{-}10}$ organic acids, diacids, and its derivates. Typical species include $C_9H_{16}O_4I^-$ (m/z 315.01, iodide adduct, probably azelaic acid **Figure S6.37**), $C_9H_{18}O_4I^-$ (m/z 317.03, iodide adduct, possibly dihydroxy or hydroperoxyl C_9 carboxylic acid), and $C_{10}H_{18}O_4I^-$ (m/z 329.03, iodide adduct, possibly sebacic, **Figure S6.38**). Highly oxygenated species with 5 oxygen atoms and more are abundant in those low-volatile factors compared to intermediate-oxidative state factors, including $C_{10}H_{18}O_5I^-$ (m/z 329.03, iodide adduct, possibly C_{10} hydroperoxyl carboxylic acid, **Figure S6.39**) and $C_9H_{16}O_5I^-$ (m/z 329.03, iodide adduct, possibly C_9 hydroperoxyl carboxylic acid, **Figure S6.40**)possibly corresponding to hydroperoxyl deviates of carboxylic acids(Zhou et al., 2022; Takhar et al., 2022; Grebenteuch et al., 2021; Yao et al., 2024). Highly-oxygenate products $C_{16/18}H_{30\text{-}34}O_{\geq 5}$ (**Figure S6.35-36**)are auto-oxidation products that keep long-chain fatty acid structure, abundant in factor LV-Multigen-HMW(Shilling et al., 2019; Takhar et al., 2019; Patrikios et al., 1994; Du et al., 2025).These larger molecule multi-generation auto-oxidation products have similar or slightly higher oxidative state and lower saturation vapor pressure, thus are more abundant in the aerosol phase.

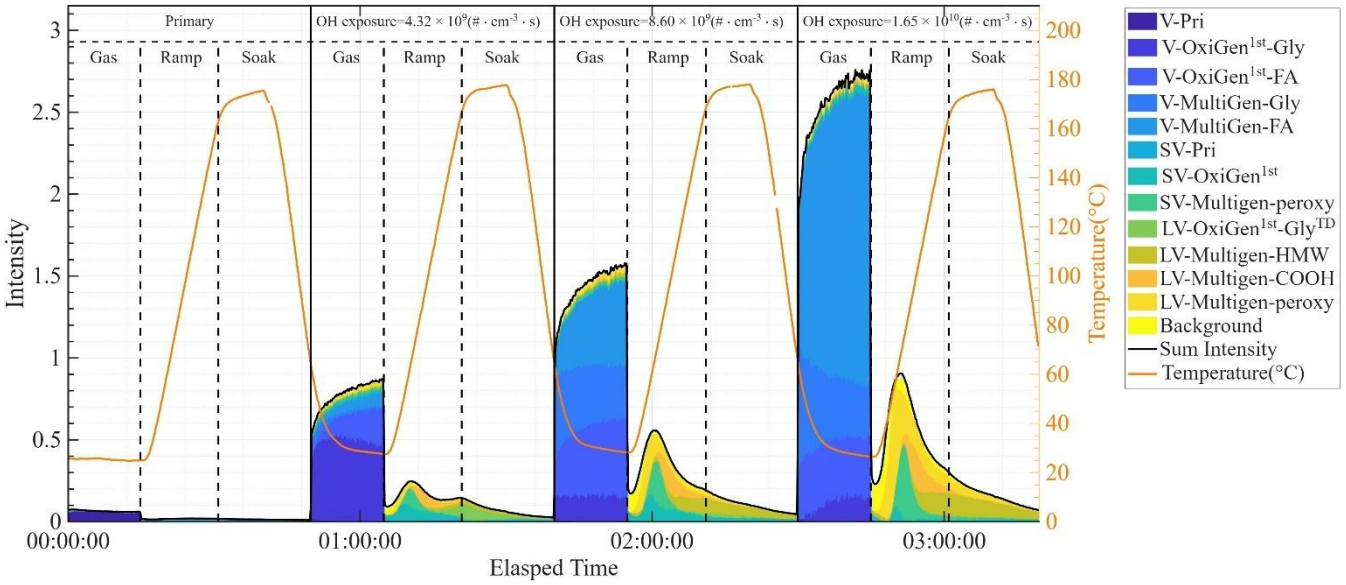

Figure 3 Factor time series of ME-2 PMF classification result with strengthen of OH exposure. Y-axis Intensity represents the sum of CIMS organic signal normalized to iodide ion other than formic acid.

3.4 Gas-particle partitioning of typical species.

Gas-particle partitioning is governed by both thermodynamic and kinetic processes. We compared characteristic time scales (τ) for gas-phase diffusion, surface desorption, and particle-phase diffusion with the time scales for particle coagulation, oxidation of cooking precursors (e.g., oleic acid), and residence in the Go:PAM. Detailed equations are provided in Section S5 of Supplement S1, and the results are shown in Figure 4. Particle-phase diffusion is the fastest modelled process in both primary and secondary aerosols across the investigated OH exposures, with τ values of approximately 10^{-2}–10^{0} s, substantially shorter than the 55 s residence time and the oxidation time scale of primary precursors, implying minor resistance of particle-phase diffusion on gas-particle partitioning under the modelled conditions. Gas-phase diffusion in the primary aerosol is partly limited by the low particle number concentration and has a characteristic time scale of approximately 10^{2} s, thus would serve as the main cause of deviation from equilibrium. In the secondary aerosol, gas-phase diffusion remains significant faster than the oxidation and residence time scales resulting in minor kinetic resistance. Surface-desorption time scales increase drastically with molecular weight: species with molecular weight >200 g mol^{-1} have desorption times longer than the residence time and account for approximately 10% of the total detected mass, whereas species with molecular weight >300 g mol^{-1} have desorption times longer than 1 h and account for approximately 5%. Surface desorption may therefore retain a limited fraction of high-molecular-weight compounds. $C_{>9}O_{>5}$ peroxides and auto oxidation products keeping long-chain fatty acid structures ($C_{16,18}O_{>4}$) would be confined to remain at aerosol phase due to kinetic limits in surface desorption process. Meanwhile, its influence on semi- and intermediate- volatile components remains minor. Faster gas-phase and aerosol phase diffusion than coagulation is in consistent with conclusions shown in Section 3.1 that dominate SOA growth driving force is condensation. It should be noticed that, adsorption onto surface have already been considered in gas-phase time scale of gas-phase diffusion processes, utilizing the effective mass accommodation coefficient α_{eff} recommended by Shiraiwa et al.(Shiraiwa and Pöschl, 2021). Varying the mass accommodation coefficient from 1 to 10^{-4} has only a minor effect on the time scales (**Figure 4 and Figures S6.46-6.47**), thus strengthen the evidence on liquid-like aerosol phase of secondary cooking aerosol (Lbadaoui-Darvas et al., 2021; Knopf et al., 2024). Varying the mass accommodation coefficient from 1 to 10^{-4} has only a minor effect on the time scales (**Figure 4 and Figures S6.46-6.47**), thus strengthen the evidence on liquid-like aerosol phase of secondary cooking aerosol. Thus, we imply that equilibrium partitioning would be somehow reasonable for secondary cooking aerosols with OH exposure below 10^{10} #·cm^{-3}·s. Results on viscosity estimation based on various methods shown in **Figure S6.45** imply a liquid-like primary and secondary cooking aerosol regardless of estimation methods, which confirms the near-equilibrium partitioning characteristics of cooking aerosols. Results are comparable to previous studies on primary and secondary cooking aerosol under the studied OH-exposure range (<10^{10} molecules cm^{-3} s)(Takhar et al., 2021; Masoud et al., 2022; Hou et al., 2025; Liu et al., 2025).

Fickian diffusion and the fractional Stokes-Einstein relationship can undergo violation in secondary organic aerosol, especially for small molecules in in highly-oxidized aerosol(Marshall et al., 2016; Bedoya-Lora et al., 2019; Evoy et al., 2021; Mutneja and Karmakar, 2025). e Deborah number and Maxwell-Stefan diffusion coefficients are calculated and utilized to

evaluated their applicability, as described in Section S5 of Supplement S1. (Preston and Zuend, 2022), as shown in **S5 of Supplement 1**. Results are shown in Figures **S6.42-6.44** of Supplement S1. he results in Figures S6.42-S6.44 indicate that deviations from the fractional Stokes-Einstein relationship and Fick's law are not expected to control the kinetics of the primary or secondary cooking aerosol under the investigated conditions (Pastore et al., 2021; Evoy et al., 2021; Preston, 2022).

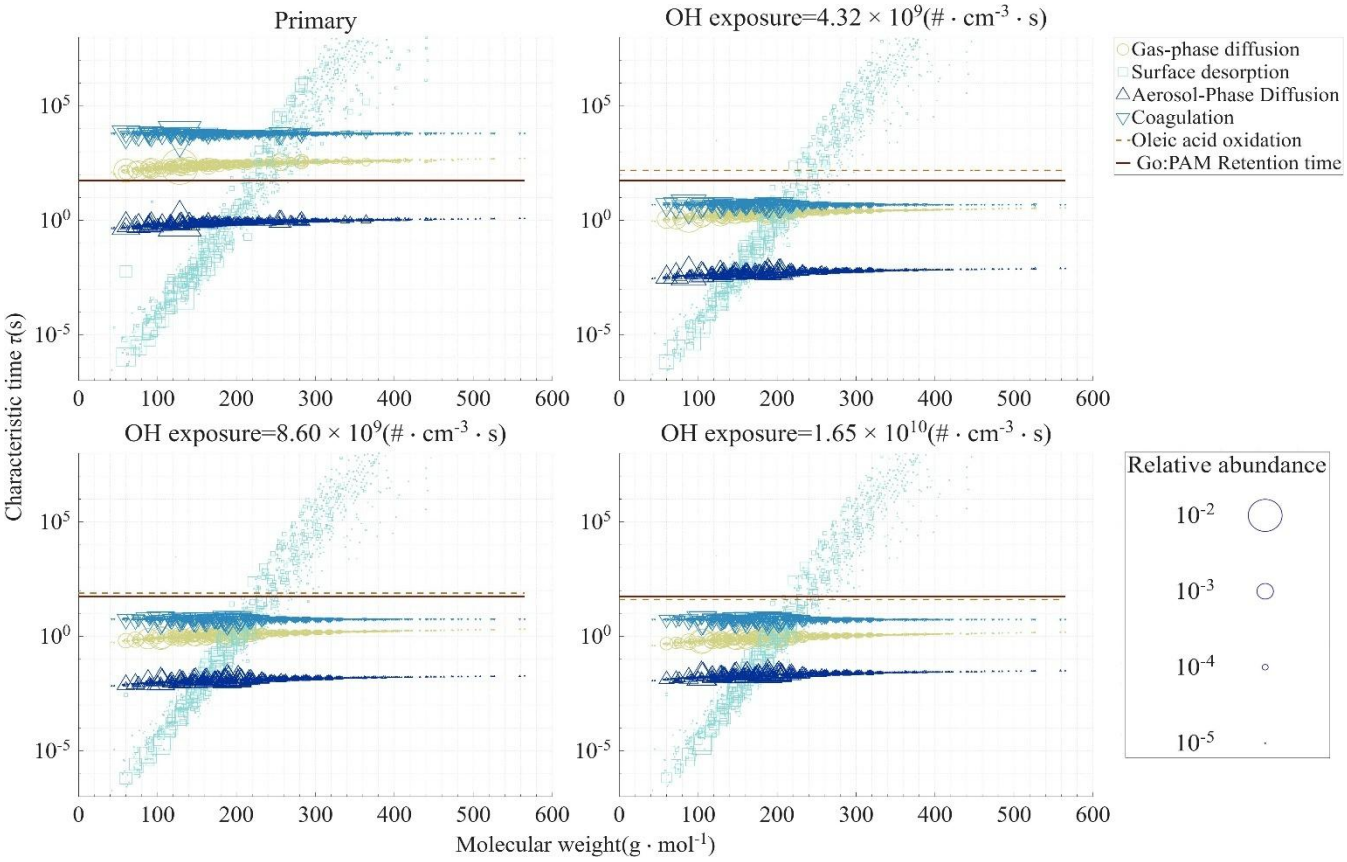

Figure 4 The characteristic time scale of FIGAERO-CIMS detected species in various kinetic transport processes of gas-particle partitioning with enhancement of OH exposure. Markers show time scale of gas-phase diffusion(circle), surface desorption(square), aerosol-phase diffusion(triangle), coagulation (reverse triangle). Lines shows reference time scale, including retention time(solid) and oleic acid oxidation(dashed). Marker size represents relative abundance of species. Surface mass accommodation coefficients are chosen to be unity.

Figure 5 compares estimated and measured volatilities of species in cooking aerosol after accounting for activity coefficients and the Kelvin effect. Liquid-liquid phase separation (LLPS) was also considered and was not predicted under the modeled conditions because none of the species had a particle-phase activity near or above unity (**Figure S6.41)**. Volatility derived from the FIGAERO particle-phase fraction and thermogram peak temperature are generally low and distributed more narrowly than the theoretical estimates. Specifically, based on FIGAERO measurements, the theory overestimates the volatility of the most abundant SVOC to IVOC species by 1-3 order of magnitude, while underestimate the volatility of LVOCs. These gaps

are higher for IVOC and LVOC, while closer at the boundary of SVOC to IVOC. Possible explanations on discrepancies between measurement and parametrization include instrumentation limits in FIGAERO measurements, such as hindered evaporation and desorption caused by the FIGAERO filter microstructure (Ylisirniö et al., 2021; Ylisirniö et al., 2025). Another possible cause might be aerosol microstructure influence of functionalized auto-oxidation product or uncertainty on activity coefficients(Wang et al., 2026; Zhang et al., 2024; Chen et al., 2025). Sensitivity test has been done by adding long-chain-fatty-acid related species into measurement result to observe the difference of thermodynamics and kinetics (**Figures S6.50-51**), showing potential underestimation would not interfere thermodynamic and kinetic estimations, indicating minor effect of fatty-acid-related instrument sensitivity.

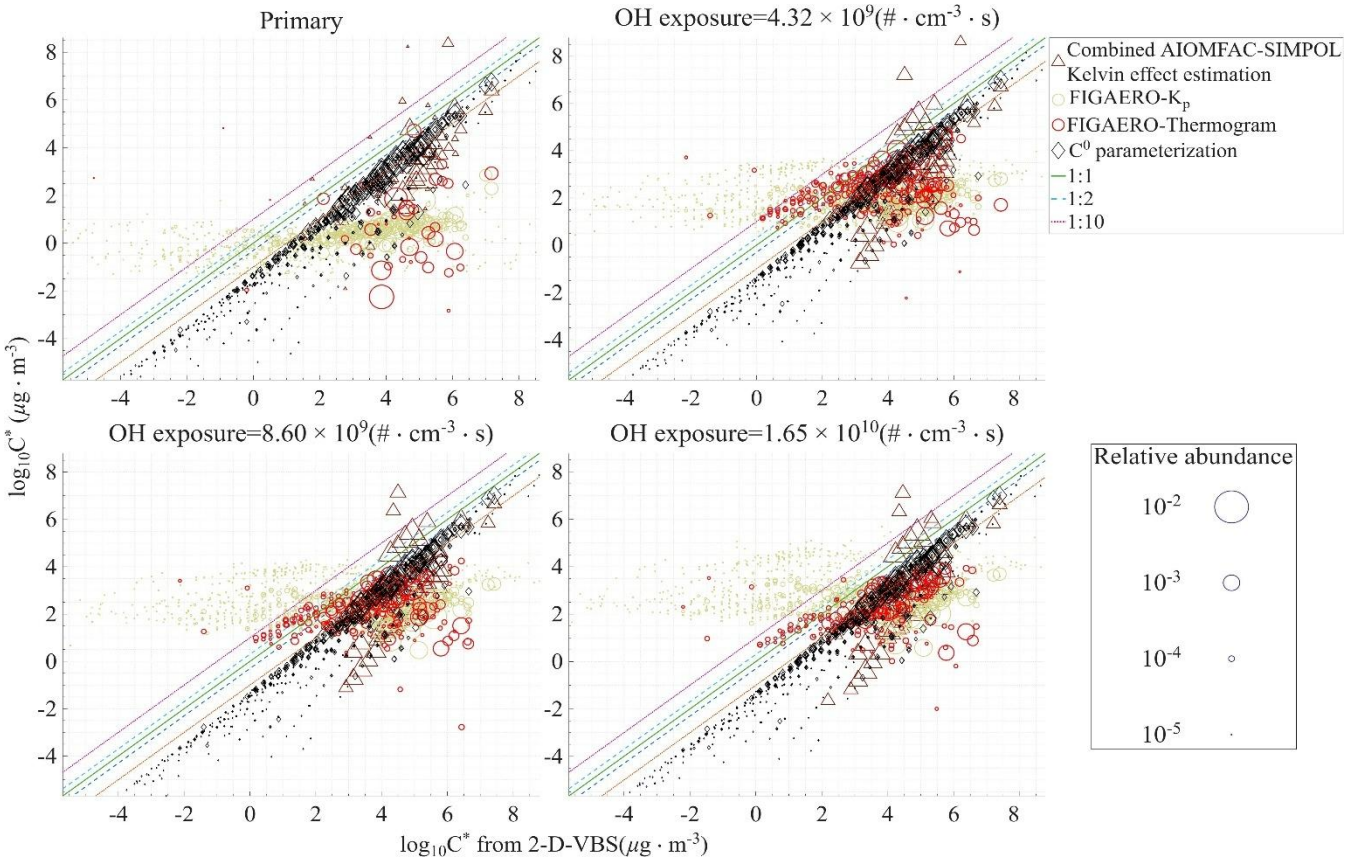

Figure 5 The characteristic effective saturated concentration C^* of FIGAERO-CIMS detected species utilizing different estimation methods with enhancement of OH exposure. Markers show combined AIOMFAC-SIMPOL vapor-pressure and activity coefficient estimation methods accounting for kelvin effect (triangle), K_p from FIGAERO measurements (yellow circle), T_{max} from FIGAERO thermograms (red circle), C^* parametrization(West et al., 2023) (reverse triangle). Lines shows 1:1,1:2 and 1:10 position. Marker size represents relative abundance of species.

To achieve more comprehensive and detailed knowledge on thermodynamic properties and influence on gas-paticle partitioning, we select typical species from ME-2 PMF factors using ordinal analysis method. Most abundant species in each

factor representing different oxidative state, volatility and precursor type are shown in Tables **S6.1-6.12** in Supplement S1. We further select the most representative species and list them in **Table 2.** Among species in **Table 2**, highly-volatile low-molecular-weight compounds, such as formic acid and acetic acid, are typically volatile organic aerosol species. The abundance of these volatile species detected in "aerosol phase" are probably resulting from thermal decomposition. We would then mainly focus on semi-volatile and low-volatile species with considerable gas-particle partitioning influence on SOA formation and evolution. These key species, including primary species related to cooking emissions(Reyes-Villegas et al., 2018), intermediate oxidative state species related to first-generation oxidation or thermal oxidation(Takhar et al., 2022), and multi-generation termination oxidation products(Masoud et al., 2022; Brown et al., 2021; Takhar et al., 2021), are listed in **Table 2**.

Table 2 Classified typical species at various oxidative state

Oxidative state	Volatility	Formula	Possible species	p^0(Pa,25°C)
Primary	Semi-volatile	$C_3H_8O_3$	Glycerol	2.24×10^{-2}
		$C_{16}H_{32}O_2$	Palmitic acid	2.67×10^{-5}
		$C_{18}H_{34}O_2$	Oleic acid	1.12×10^{-4}
First-generation	Semi-volatile	$C_3H_4O_3$	Pyruvic acid	1.72×10^{2}
		$C_7H_{12}O_3$	-	1.18×10^{0}
		$C_{10}H_{16}O_3$	-	1.09×10^{-1}
	Low-volatile	$C_{16}H_{32}O_3$	-	6.96×10^{-6}
Multi-generations	Semi-volatile	$C_4H_6O_4$	Succinic acid	1.04×10^{-3}
		$C_6H_{10}O_4$	Adipic acid	5.4×10^{-4}
		$C_9H_{16}O_4$	Azelaic acid	4.74×10^{-5}
	Low-volatile	$C_{10}H_{18}O_5$	-	4.02×10^{-5}
		$C_{18}H_{32}O_6$	-	1.39×10^{-8}

Figure 6 summarized the gas-particle partitioning of typical species chosen in **Table 2**, representing gas-particle partitioning characteristics of species with enhancing oxidative exposure, illustrating the discrepancies between estimated and experimental values of the partitioning coefficient (K_p) for typical components at varying oxidation degrees as the oxidation process progresses. The subplot legends indicate the oxidation degree of each component, where dashed lines represent estimated values and solid lines denote experimental values. Specifically, among primary emission components, the gas-particle partitioning of typical species deviate toward aerosol phase, due to limitations on gas-phase diffusion mentioned before. With oxidation proceeds leading to SOA formation, the partitioning coefficient of primary components decreases significantly closer to theoretical values, indicating SOA formation would relieve the gas-phase diffusion limit and thus consumption of primary components push the gas-particle partitioning toward equilibrium. Among first-generation oxidation products, components with $C_{\geq5}$ primarily originating from fatty acid cleavage are predominate, while a minority of $C_{\leq4}$ components derive from glycerol oxidation existed. The theoretical K_p values for $C_{\geq5}$ first-generation oxidation products generated via scissoring

reactions are markable lower than FIGAERO-measured values, indicating a substantial deviation from equilibrium in their gas-particle partitioning. Functionalized multi-generation oxidation products from scissoring of long-chain fatty acids including exhibit lesser deviation from estimated, possibly due to its structure similarity with aerosol bulk composition; However, large molecule oxidation products ($C_{\geq 12}O_{\geq 5}$, e.g., $C_{18}H_{32}O_6$) demonstrate significant deviations. Estimates based on equilibrium partitioning suggest that these components should only occupy a minimal fraction in the gas phase; however, measurement results in substantial gas-phase presence, consistent with general results shown in **Figure 5.**

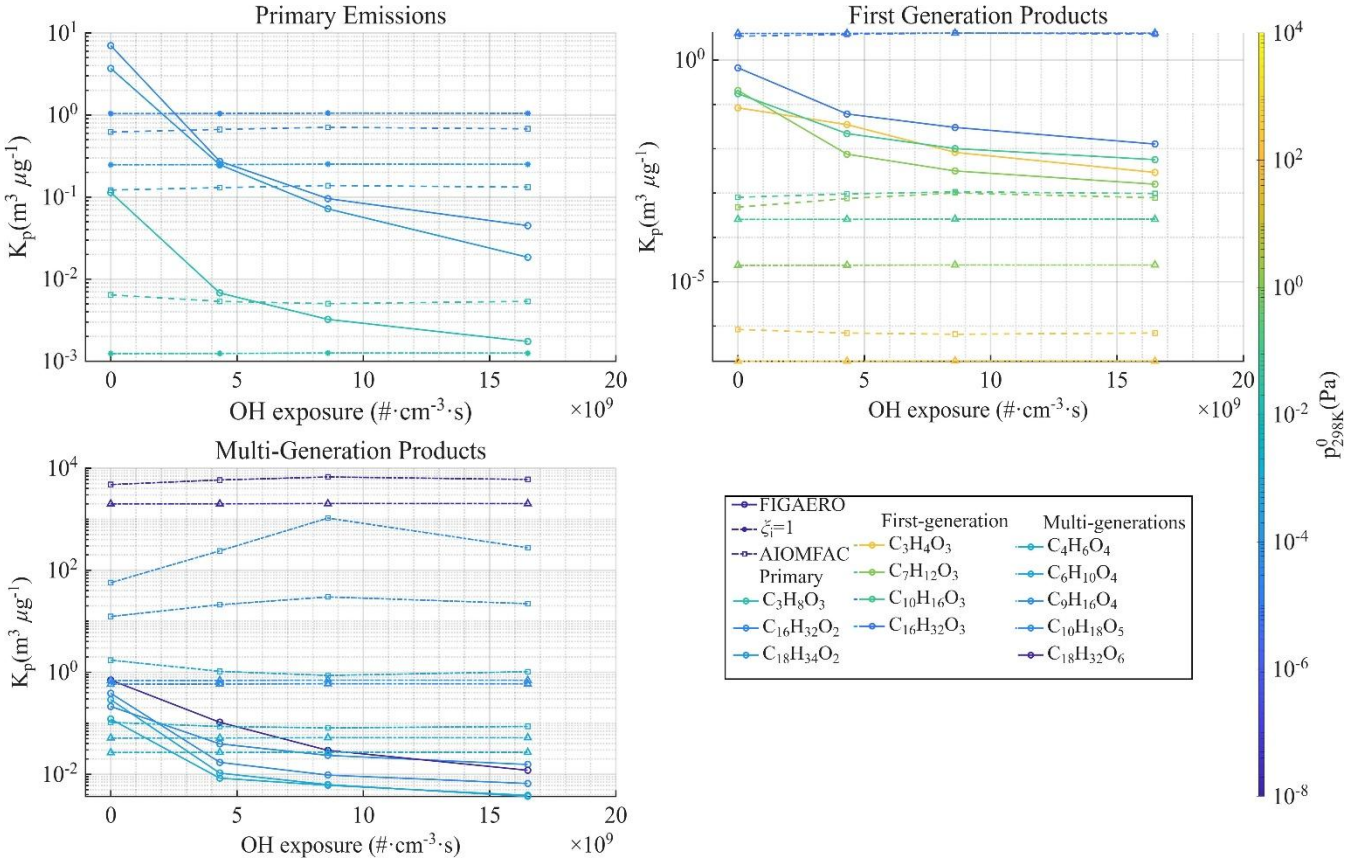

Figure 6 measurement and estimated partitioning coefficient (K_p) evolution of typical species of (a) primary emission (b) first generation products (c) multi-generation oxidation products

Overall, the gas-particle partitioning inferred for medium-molecular-weight, moderately oxidized compounds ($C_{3-8}O_{3-4}$) and highly oxidized large molecules ($C_{\geq 12}O_{\geq 5}$) differs from the idealized equilibrium estimates. The theoretical approach overestimates K_p for the $C_{3-8}O_{3-4}$ group and underestimates K_p for the $C_{\geq 12}O_{\geq 5}$ group. These deviations should not be assigned to a single process. Non-ideal thermodynamics, including composition-dependent activity coefficients, can alter partitioning relative to an ideal organic solution. The kinetic calculations further indicate that particle-phase diffusion is too fast to be the dominant resistance under the modeled conditions, although gas-phase transport in the low-number-concentration primary aerosol and surface desorption of a limited high-molecular-weight fraction may contribute. In addition, uncertainties in pure-

component vapor pressures, activity coefficients, FIGAERO quantification, filter-mediated desorption, and thermal decomposition or rearrangement can affect the comparison. We therefore interpret the compound-class differences as a combined thermodynamic, kinetic, and measurement-model discrepancy rather than as direct evidence of particle-phase (Shiraiwa et al., 2012; Zhang et al., 2012; Zaveri et al., 2018). In contrast, for high-oxidative-state large molecules, diffusion and surface mass transfer limitations impede their entry into the particle phase, resulting in their persistence in the gas phase(Zaveri et al., 2018; Masoud et al., 2022; Schervish and Shiraiwa, 2023). As an intrinsic property of FIGAERO-CIMS instrumentation, thermal desorption related measurement uncertainties, including thermal decomposition, may also contribute to the observed deviations(Mehra et al., 2020; Tikkanen et al., 2020; Masoud et al., 2022). The gap remains the crucial challenge in gas-particle partitioning studies, here we descript the phenomenon in a rigorous way.

4 Conclusion

This study presents a comprehensive investigation into the atmospheric evolution of cooking-derived organic aerosols, integrating advanced analytical techniques to unravel complex gas-particle dynamics. By deploying a Go:PAM flow tube oxidation system coupled with FIGAERO-I-CIMS, we quantitatively tracked changes in chemical composition, volatility, and gas-particle partitioning throughout oxidation. A key innovation lies in the combined application of high-resolution mass spectrometry with a two-dimensional volatility basis set (2-D VBS) framework, enabling a mechanistic understanding of composition-dependent partitioning behavior.

Under typical atmospheric conditions, primary cooking emissions rapidly generated substantial quantities of fine particles (~10 nm) within two hours, followed by the formation of higher concentrations of 30–50 nm secondary aerosols over 0.5-1 days. Notably, oxidation products predominantly occupied the semi-volatile and intermediate-volatility organic compounds (S/IVOCs) range in the 2-D VBS, systematically migrating toward the SVOC region as oxidation progressed, while molecular weight and oxidation degree remained relatively stable. Leveraging positive matrix factorization (PMF), we systematically classified compounds by oxidation degree and volatility, identifying representative markers across evolution stages: gaseous glycerol and particulate long-chain fatty acids in primary emissions; medium-weight carbonyl acids (e.g., $C_5H_{10}O_3$, $C_7H_{12}O_3$) as intermediate products, and multi-generation oxidation products including dicarboxylic acids (e.g., $C_9H_{16}O_4$) and HOM-like compounds (e.g., $C_{18}H_{32}O_{5–6}$) as mature products. Of particular importance are highly oxidized small organic acids ($\leq C_3$) and multi-generation products in the C_7-C_{10} range with moderate volatility and high oxidation state.

A central finding concerns the thermodynamics and kinetics gas-particle partitioning observed across different compound classes. Observation shows that scission-derived functionalized multi-generation oxidation products approached theoretical equilibrium, and identified significant kinetic limitations for first-generation oxidation products ($C_{3–8}O_{3–4}$) and large non-cleavage products ($>C_{14}O_5$), which exhibited significant deviations. Based on comprehensive estimation and parametrization of kinetic and thermodynamic processes, we concluded that the secondary cooking aerosol in this study are near equilibrium state for most S/IVOCs that are predominant in this study, while partitioning in primary aerosols are constrained by gas-phase

diffusion, and surface desorption account for most diffusion limit of large non-cleavage products (>$C_{14}O_5$). Thermodynamic analysis unravels gap between theory and measurements especially for small and large molecules, requiring further instrumentation and theory development. The mechanistic insight into partitioning dynamics represents a significant advance in understanding the atmospheric behavior of cooking emissions. Our results provide a scientific foundation for refining emission inventories and air quality models, ultimately contributing to improved exposure assessment and mitigation strategies for urban and indoor environments.

Code, data, or code and data availability

Data are available upon request.

Supplement link

Supplementary material is available in the online version of this article.

Author contributions

SG, MH design the research, RS, HW, YY, WZ, ZC, RT, SC perform the experiment, SG, ZW, SL, YC, MH supervise the research, SG provide the research funding, RS, HW, YY analysis the data, RS, SG write the original draft the the manuscript, all the authors review and edit the final manuscript.

Competing interests

Authors declare no competing interests.

Acknowledgements

This research was supported by the National Key R&D Program of China (2022YFC3701000, Task 2), National Natural Science Foundation of China-Creative Research Group Fund (22221004).

References

Abdullahi, K. L., Delgado-Saborit, J. M., and Harrison, R. M.: Emissions and indoor concentrations of particulate matter and its specific chemical components from cooking: A review, Atmospheric Environment, 71, 260-294, 10.1016/j.atmosenv.2013.01.061, 2013.

Aladedunye, F.: Toxic contaminants of thermo-oxidatively processed edible oils/fats, Lipid Technol., 28, 117-121, 10.1002/lite.201600032, 2016.

Atkinson, R., Baulch, D. L., Cox, R. A., Crowley, J. N., Hampson, R. F., Hynes, R. G., Jenkin, M. E., Rossi, M. J., Troe, J., and Subcommittee, I.: Evaluated kinetic and photochemical data for atmospheric chemistry: Volume II – gas phase reactions of organic species, Atmos. Chem. Phys., 6, 3625-4055, 10.5194/acp-6-3625-2006, 2006.
Bandowe, B. A. M., Lui, K. H., Jones, T., BeruBe, K., Adams, R., Niu, X., Wei, C., Cao, J. J., Lee, S. C., Chuang, H. C., and Ho, K. F.: The chemical composition and toxicological effects of fine particulate matter (PM(2.5)) emitted from different cooking styles, Environ Pollut, 288, 117754, 10.1016/j.envpol.2021.117754, 2021.
Bannan, T. J., Le Breton, M., Priestley, M., Worrall, S. D., Bacak, A., Marsden, N. A., Mehra, A., Hammes, J., Hallquist, M., Alfarra, M. R., Krieger, U. K., Reid, J. P., Jayne, J., Robinson, W., McFiggans, G., Coe, H., Percival, C. J., and Topping, D.: A method for extracting calibrated volatility information from the FIGAERO-HR-ToF-CIMS and its experimental application, Atmospheric Measurement Techniques, 12, 1429-1439, 10.5194/amt-12-1429-2019, 2019.
Bedoya-Lora, F. E., Echeverria, F., and Calderon, J. A.: Effectiveness of non-Fickian diffusion model on the water uptake determination of different organic coatings, Progress in Organic Coatings, 136, 10.1016/j.porgcoat.2019.06.052, 2019.
Bonetti, R. and Parker, W. O.: Insights into Polymerization of Vegetable Oil: Oligomerization of Oleic Acid, JAOCS J Am Oil Chem Soc, 96, 1181-1184, 10.1002/aocs.12274, 2019.
Brown, W. L., Day, D. A., Stark, H., Pagonis, D., Krechmer, J. E., Liu, X., Price, D. J., Katz, E. F., DeCarlo, P. F., Masoud, C. G., Wang, D. S., Hildebrandt Ruiz, L., Arata, C., Lunderberg, D. M., Goldstein, A. H., Farmer, D. K., Vance, M. E., and Jimenez, J. L.: Real-time organic aerosol chemical speciation in the indoor environment using extractive electrospray ionization mass spectrometry, Indoor Air, 31, 141-155, 10.1111/ina.12721, 2021.
Buchholz, A., Ylisirniö, A., Huang, W., Mohr, C., Canagaratna, M., Worsnop, D. R., Schobesberger, S., and Virtanen, A.: Deconvolution of FIGAERO–CIMS thermal desorption profiles using positive matrix factorisation to identify chemical and physical processes during particle evaporation, Atmos. Chem. Phys., 20, 7693-7716, 10.5194/acp-20-7693-2020, 2020a.
Buchholz, A., Ylisirniö, A., Huang, W., Mohr, C., Canagaratna, M., Worsnop, D. R., Schobesberger, S., and Virtanen, A.: Deconvolution of FIGAERO-CIMS thermal desorption profiles using positive matrix factorisation to identify chemical and physical processes during particle evaporation, Atmospheric Chemistry and Physics, 20, 7693-7716, 10.5194/acp-20-7693-2020, 2020b.
Cai, X. and Griffin, R. J.: Modeling the formation of secondary organic aerosol in coastal areas: Role of the sea-salt aerosol organic layer, Journal of Geophysical Research: Atmospheres, 108, 10.1029/2002JD003053, 2003.
Canonaco, F., Crippa, M., Slowik, J. G., Baltensperger, U., and Prévôt, A. S. H.: SoFi, an IGOR-based interface for the efficient use of the generalized multilinear engine (ME-2) for the source apportionment: ME-2 application to aerosol mass spectrometer data, Atmospheric Measurement Techniques, 6, 3649-3661, 10.5194/amt-6-3649-2013, 2013.
Chandramouli, B., Jang, M., and Kamens, R. M.: Gas–particle partitioning of semi-volatile organics on organic aerosols using a predictive activity coefficient model: analysis of the effects of parameter choices on model performance, Atmospheric Environment, 37, 853-864, 10.1016/s1352-2310(02)00931-7, 2003.
Chen, Y., Xia, M., Zheng, P., Li, Y., Zou, Z., Tong, S., Li, K., Feng, X., Hui, L., Yuan, Q., Li, J., Yu, J. Z., Lee, S., Wang, T., and Wang, Z.: Complex gas-particle partitioning of nitro-phenolic compounds: field-based insights and determination of apparent activity coefficient, npj Climate and Atmospheric Science, 8, 10.1038/s41612-025-01156-z, 2025.
Chiaia, V., Micalizzi, G., Donnarumma, D., Irto, A., Bretti, C., Venuti, M., Lando, G., Mondello, L., and Cardiano, P.: Study of oxidation products in aged olive oils by GC and HPLC techniques coupled to mass spectrometry to discriminate olive oil lipid substances in archaeological artifacts from ancient Taormina (Italy), Journal of Chromatography A, 1731, 10.1016/j.chroma.2024.465154, 2024.
Chuang, W. K. and Donahue, N. M.: A two-dimensional volatility basis set – Part 3: Prognostic modeling and NOx dependence, Atmospheric Chemistry and Physics, 16, 123-134, 10.5194/acp-16-123-2016, 2016.
Donahue, N. M., Epstein, S. A., Pandis, S. N., and Robinson, A. L.: A two-dimensional volatility basis set: 1. organic-aerosol mixing thermodynamics, Atmospheric Chemistry and Physics, 11, 3303-3318, 10.5194/acp-11-3303-2011, 2011.
Donahue, N. M., Kroll, J. H., Pandis, S. N., and Robinson, A. L.: A two-dimensional volatility basis set – Part 2: Diagnostics of organic-aerosol evolution, Atmospheric Chemistry and Physics, 12, 615-634, 10.5194/acp-12-615-2012, 2012.
Du, Y., Che, H., Bao, Z., Liu, Y., Li, Q., Hu, M., Zhou, J., Zhang, S., Yao, X., Shi, Q., Chen, C., Han, Y., Meng, L., Long, X., Qi, X., He, C., and Chen, Y.: Evolution of atmospheric high-molecular-weight Organonitrates (HMW ONs) in urban Yangtze River Delta (YRD), China, npj Climate and Atmospheric Science, 8, 10.1038/s41612-025-00928-x, 2025.

Evoy, E., Kiland, K. J., Huang, Y., Schnitzler, E. G., MacLean, A. M., Kamal, S., Abbatt, J. P. D., and Bertram, A. K.: Diffusion Coefficients and Mixing Times of Organic Molecules in β-Caryophyllene Secondary Organic Aerosol (SOA) and Biomass Burning Organic Aerosol (BBOA), ACS Earth and Space Chemistry, 5, 3268-3278, 10.1021/acsearthspacechem.1c00317, 2021.

Farmer, D. K., Vance, M. E., Abbatt, J. P. D., Abeleira, A., Alves, M. R., Arata, C., Boedicker, E., Bourne, S., Cardoso-Saldana, F., Corsi, R., DeCarlo, P. F., Goldstein, A. H., Grassian, V. H., Hildebrandt Ruiz, L., Jimenez, J. L., Kahan, T. F., Katz, E. F., Mattila, J. M., Nazaroff, W. W., Novoselac, A., O'Brien, R. E., Or, V. W., Patel, S., Sankhyan, S., Stevens, P. S., Tian, Y., Wade, M., Wang, C., Zhou, S., and Zhou, Y.: Overview of HOMEChem: House Observations of Microbial and Environmental Chemistry, Environ Sci Process Impacts, 21, 1280-1300, 10.1039/c9em00228f, 2019.

Frankel, E. N., Neff, W. E., and Selke, E.: Analysis of autoxidized fats by gas chromatography-mass spectrometry: VIII. Volatile thermal decomposition products of hydroperoxy cyclic peroxides, Lipids, 18, 353-357, 10.1007/BF02537231, 1983.

Grebenteuch, S., Kroh, L. W., Drusch, S., and Rohn, S.: Formation of secondary and tertiary volatile compounds resulting from the lipid oxidation of rapeseed oil, Foods, 10, 10.3390/foods10102417, 2021.

Guo, S., Hu, M., Peng, J., Wu, Z., Zamora, M. L., Shang, D., Du, Z., Zheng, J., Fang, X., Tang, R., Wu, Y., Zeng, L., Shuai, S., Zhang, W., Wang, Y., Ji, Y., Li, Y., Zhang, A. L., Wang, W., Zhang, F., Zhao, J., Gong, X., Wang, C., Molina, M. J., and Zhang, R.: Remarkable nucleation and growth of ultrafine particles from vehicular exhaust, P Natl Acad Sci USA, 117, 3427-3432, 10.1073/pnas.1916366117, 2020.

Guo, Z., Chen, X., Wu, D., Huo, Y., Cheng, A., Liu, Y., Li, Q., and Chen, J.: Higher Toxicity of Gaseous Organics Relative to Particulate Matters Emitted from Typical Cooking Processes, Environmental Science & Technology, 57, 17022-17031, 10.1021/acs.est.3c05425, 2023.

Hallquist, M., Wenger, J. C., Baltensperger, U., Rudich, Y., Simpson, D., Claeys, M., Dommen, J., Donahue, N. M., George, C., Goldstein, A. H., Hamilton, J. F., Herrmann, H., Hoffmann, T., Iinuma, Y., Jang, M., Jenkin, M. E., Jimenez, J. L., Kiendler-Scharr, A., Maenhaut, W., McFiggans, G., Mentel, T. F., Monod, A., Prévôt, A. S. H., Seinfeld, J. H., Surratt, J. D., Szmigielski, R., and Wildt, J.: The formation, properties and impact of secondary organic aerosol: current and emerging issues, Atmos. Chem. Phys., 9, 5155-5236, 10.5194/acp-9-5155-2009, 2009.

Hashimoto, S., Takazawa, Y., Ieda, T., Omagari, R., Nakajima, D., Nakamura, S., and Suzuki, N.: Application of rapid air sampling and non-targeted analysis using thermal desorption comprehensive two-dimensional gas chromatography/time-of-flight mass spectrometry to accidental fire, Chemosphere, 303, 10.1016/j.chemosphere.2022.135021, 2022.

He, L.-Y., Hu, M., Huang, X.-F., Yu, B.-D., Zhang, Y.-H., and Liu, D.-Q.: Measurement of emissions of fine particulate organic matter from Chinese cooking, Atmospheric Environment, 38, 6557-6564, 10.1016/j.atmosenv.2004.08.034, 2004.

Hou, S., Liu, W., and Kuwata, M.: Fresh Cooking Organic Aerosol Particles Exist as Liquid in Most Urban Temperature Range, Journal of Geophysical Research: Atmospheres, 130, 10.1029/2025JD043825, 2025.

Iyer, S., Lopez-Hilfiker, F., Lee, B. H., Thornton, J. A., and Kurten, T.: Modeling the Detection of Organic and Inorganic Compounds Using Iodide-Based Chemical Ionization, J Phys Chem A, 120, 576-587, 10.1021/acs.jpca.5b09837, 2016.

Kawada, T., Krishnamurthy, R. G., Mookherjee, B. D., and Chang, S. S.: Chemical reactions involved in the deep fat frying of foods. II. Identification of acidic volatile decomposition products of corn oil, Journal of the American Oil Chemists' Society, 44, 131-135, 10.1007/BF02558172, 1967.

Knopf, D. A., Ammann, M., Berkemeier, T., Pöschl, U., and Shiraiwa, M.: Desorption lifetimes and activation energies influencing gas–surface interactions and multiphase chemical kinetics, Atmospheric Chemistry and Physics, 24, 3445-3528, 10.5194/acp-24-3445-2024, 2024.

Kong, X., Salvador, C. M., Carlsson, S., Pathak, R., Davidsson, K. O., Le Breton, M., Gaita, S. M., Mitra, K., Hallquist, A. M., Hallquist, M., and Pettersson, J. B. C.: Molecular characterization and optical properties of primary emissions from a residential wood burning boiler, Sci Total Environ, 754, 142143, 10.1016/j.scitotenv.2020.142143, 2021.

Kristensen, K., Lunderberg, D. M., Liu, Y., Misztal, P. K., Tian, Y., Arata, C., Nazaroff, W. W., and Goldstein, A. H.: Gas–Particle Partitioning of Semivolatile Organic Compounds in a Residence: Influence of Particles from Candles, Cooking, and Outdoors, Environmental Science & Technology, 57, 3260-3269, 10.1021/acs.est.2c07172, 2023.

Lbadaoui-Darvas, M., Takahama, S., and Nenes, A.: Molecular-scale description of interfacial mass transfer in phase-separated aqueous secondary organic aerosol, Atmospheric Chemistry and Physics, 21, 17687-17714, 10.5194/acp-21-17687-2021, 2021.

Le Breton, M., Psichoudaki, M., Hallquist, M., Watne, Å. K., Lutz, A., and Hallquist, Å. M.: Application of a FIGAERO ToF CIMS for on-line characterization of real-world fresh and aged particle emissions from buses, Aerosol Science and Technology, 53, 244-259, 10.1080/02786826.2019.1566592, 2019.

Lee, B. H., Lopez-Hilfiker, F. D., Mohr, C., Kurten, T., Worsnop, D. R., and Thornton, J. A.: An Iodide-Adduct High-Resolution Time-of-Flight Chemical-Ionization Mass Spectrometer: Application to Atmospheric Inorganic and Organic Compounds, Environmental Science & Technology, 48, 6309-6317, 10.1021/es500362a, 2014.

Li, Y.-C., Shu, M., Ho, S. S. H., Wang, C., Cao, J.-J., Wang, G.-H., Wang, X.-X., Wang, K., and Zhao, X.-Q.: Characteristics of PM2.5 emitted from different cooking activities in China, Atmospheric Research, 166, 83-91, 10.1016/j.atmosres.2015.06.010, 2015.

Li, Y., Pöschl, U., and Shiraiwa, M.: Molecular corridors and parameterizations of volatility in the chemical evolution of organic aerosols, Atmospheric Chemistry and Physics, 16, 3327-3344, 10.5194/acp-16-3327-2016, 2016.

Lin, C., Huang, R. J., Duan, J., Zhong, H., and Xu, W.: Polycyclic aromatic hydrocarbons from cooking emissions, Sci Total Environ, 151700, 10.1016/j.scitotenv.2021.151700, 2021.

Liu, W., He, L., Li, Y., Li, P., Chen, S., Chen, J., Liu, Y., and Kuwata, M.: Prolonged Atmospheric Chemical Lifetime of Unsaturated Fatty Acids From Cooking Sources Observed in Beijing During Wintertime, Journal of Geophysical Research: Atmospheres, 130, 10.1029/2025JD044172, 2025.

Liu, W., Zhou, L., Yuan, W., Ruan, L., Wang, X., Guo, Y., Xie, Z., Liu, Q., and Wang, C.: Tracking indoor volatile organic compounds with online mass spectrometry, TrAC Trends Anal. Chem., 171, 10.1016/j.trac.2023.117514, 2024.

Lopez-Hilfiker, F. D., Pospisilova, V., Huang, W., Kalberer, M., Mohr, C., Stefenelli, G., Thornton, J. A., Baltensperger, U., Prevot, A. S. H., and Slowik, J. G.: An extractive electrospray ionization time-of-flight mass spectrometer (EESI-TOF) for online measurement of atmospheric aerosol particles, Atmospheric Measurement Techniques, 12, 4867-4886, 10.5194/amt-12-4867-2019, 2019.

Lopez-Hilfiker, F. D., Mohr, C., Ehn, M., Rubach, F., Kleist, E., Wildt, J., Mentel, T. F., Lutz, A., Hallquist, M., Worsnop, D., and Thornton, J. A.: A novel method for online analysis of gas and particle composition: description and evaluation of a Filter Inlet for Gases and AEROsols (FIGAERO), Atmospheric Measurement Techniques, 7, 983-1001, 10.5194/amt-7-983-2014, 2014.

Lopez-Hilfiker, F. D., Mohr, C., D'Ambro, E. L., Lutz, A., Riedel, T. P., Gaston, C. J., Iyer, S., Zhang, Z., Gold, A., Surratt, J. D., Lee, B. H., Kurten, T., Hu, W. W., Jimenez, J., Hallquist, M., and Thornton, J. A.: Molecular Composition and Volatility of Organic Aerosol in the Southeastern U.S.: Implications for IEPOX Derived SOA, Environ Sci Technol, 50, 2200-2209, 10.1021/acs.est.5b04769, 2016.

Lopez-Pedrajas, S., Estevez, R., Schnee, J., Gaigneaux, E. M., Luna, D., and Bautista, F. M.: Study of the gas-phase glycerol oxidehydration on systems based on transition metals (Co, Fe, V) and aluminium phosphate, Molecular Catalysis, 455, 68-77, 10.1016/j.mcat.2018.05.020, 2018.

Lu, L., Ng, V. Y. Z., Tan, M. Z. H., Kasthuriarachchi, N. Y., Rivellini, L.-H., Tan, Y. Q., Ang, L., Viera, M., Bay, B. H., Seow, W. J., and Lee, A. K. Y.: Particle-bound reactive oxygen species in cooking emissions: Aging effects and cytotoxicity, Atmospheric Environment, 319, 10.1016/j.atmosenv.2023.120309, 2024.

Luo, Z., Zang, H., Li, Z., Li, C., and Zhao, Y.: Species-specific effect of particle viscosity and particle-phase reactions on the formation of secondary organic aerosol, Science of The Total Environment, 950, 10.1016/j.scitotenv.2024.175207, 2024.

Marshall, F. H., Miles, R. E. H., Song, Y. C., Ohm, P. B., Power, R. M., Reid, J. P., and Dutcher, C. S.: Diffusion and reactivity in ultraviscous aerosol and the correlation with particle viscosity, Chem Sci, 7, 1298-1308, 10.1039/c5sc03223g, 2016.

Martins, G. B. C., Mello, V. M., and Suarez, P. A. Z.: Thermal processes in fats and oils, Rev. Virtual Quim., 5, 16-25, 10.5935/1984-6835.20130003, 2013.

Masoud, C. G., Li, Y., Wang, D. S., Katz, E. F., DeCarlo, P. F., Farmer, D. K., Vance, M. E., Shiraiwa, M., and Hildebrandt Ruiz, L.: Molecular composition and gas-particle partitioning of indoor cooking aerosol: Insights from a FIGAERO-CIMS and kinetic aerosol modeling, Aerosol Science and Technology, 56, 1156-1173, 10.1080/02786826.2022.2133593, 2022.

Mehra, A., Krechmer, J. E., Lambe, A., Sarkar, C., Williams, L., Khalaj, F., Guenther, A., Jayne, J., Coe, H., and Worsnop, D.: Oligomer and highly oxygenated organic molecule formation from oxidation of oxygenated monoterpenes emitted by California sage plants, Atmospheric Chemistry and Physics, 20, 10953-10965, 10.5194/acp-20-10953-2020, 2020.

Milsom, A., Squires, A. M., Boswell, J. A., Terrill, N. J., Ward, A. D., and Pfrang, C.: An organic crystalline state in ageing atmospheric aerosol proxies: spatially resolved structural changes in levitated fatty acid particles, Atmospheric Chemistry and Physics, 21, 15003-15021, 10.5194/acp-21-15003-2021, 2021.
Mutneja, A. and Karmakar, S.: Length-scale dependence of Stokes-Einstein breakdown in active glass-forming liquids, Physical Review E, 111, 10.1103/PhysRevE.111.035409, 2025.
Nawar, W. W.: Thermal degradation of lipids, J Agr Food Chem, 17, 18-21, 10.1021/jf60161a012, 1969.
Nolte, C. G., Schauer, J. J., Cass, G. R., and Simoneit, B. R. T.: Highly Polar Organic Compounds Present in Meat Smoke, Environmental Science & Technology, 33, 3313-3316, 10.1021/es990122v, 1999.
Pankow, J. F.: An absorption model of the gas/aerosol partitioning involved in the formation of secondary organic aerosol, Atmospheric Environment, 28, 189-193, https://doi.org/10.1016/1352-2310(94)90094-9, 1994.
Pankow, J. F. and Asher, W. E.: SIMPOL.1: a simple group contribution method for predicting vapor pressures and enthalpies of vaporization of multifunctional organic compounds, Atmos. Chem. Phys., 8, 2773-2796, 10.5194/acp-8-2773-2008, 2008.
Pastore, R., Kikutsuji, T., Rusciano, F., Matubayasi, N., Kim, K., and Greco, F.: Breakdown of the Stokes-Einstein relation in supercooled liquids: A cage-jump perspective, Journal of Chemical Physics, 155, 10.1063/5.0059622, 2021.
Patrikios, I. S., Britton, O., Bing, D. K., and Russell, C. S.: Heating unsaturated fatty acids in air produces hemagglutinins, Biochim. Biophys. Acta Lipids Lipid Metab., 1212, 225-234, 10.1016/0005-2760(94)90257-7, 1994.
Peng, Z. and Jimenez, J. L.: Radical chemistry in oxidation flow reactors for atmospheric chemistry research, Chem Soc Rev, 49, 2570-2616, 10.1039/c9cs00766k, 2020.
Peng, Z., Day, D. A., Ortega, A. M., Palm, B. B., Hu, W., Stark, H., Li, R., Tsigaridis, K., Brune, W. H., and Jimenez, J. L.: Non-OH chemistry in oxidation flow reactors for the study of atmospheric chemistry systematically examined by modeling, Atmos. Chem. Phys., 16, 4283-4305, 10.5194/acp-16-4283-2016, 2016.
Preston, T. C.: Non-Fickian diffusion in viscous aerosol particles, Canadian Journal of Chemistry, 100, 168-174, 10.1139/cjc-2021-0187, 2022.
Preston, T. C. and Zuend, A.: Equilibration times in viscous and viscoelastic aerosol particles, Environmental Science: Atmospheres, 2, 1376-1388, 10.1039/d2ea00065b, 2022.
Qian, B., Zhu, X., Su, C., Li, H., Wu, Q., Liu, C., Pan, Y., and Han, B.: Mechanism of Water-Enhanced Volatile Aldehyde Release in Oil Fumes from Thermal Oxidation of Oleic Acid: Insights from Synchrotron Radiation Photoionization and Gas Chromatography–Mass Spectrometry, Molecules, 31, 10.3390/molecules31040594, 2026.
Reyes-Villegas, E., Bannan, T., Le Breton, M., Mehra, A., Priestley, M., Percival, C., Coe, H., and Allan, J. D.: Online Chemical Characterization of Food-Cooking Organic Aerosols: Implications for Source Apportionment, Environ Sci Technol, 52, 5308-5318, 10.1021/acs.est.7b06278, 2018.
Rogge, W. F., Hildemann, L. M., Mazurek, M. A., Cass, G. R., and Simoneit, B. R. T.: Sources of fine organic aerosol. 1. Charbroilers and meat cooking operations, Environmental Science & Technology, 25, 1112-1125, 10.1021/es00018a015, 1991.
Schervish, M. and Shiraiwa, M.: Impact of phase state and non-ideal mixing on equilibration timescales of secondary organic aerosol partitioning, Atmospheric Chemistry and Physics, 23, 221-233, 10.5194/acp-23-221-2023, 2023.
Schmedding, R., Franssen, M., and Zuend, A.: A Machine Learning Approach for Predicting the Pure-Component Surface Tension of Atmospherically Relevant Organic Compounds, ACS ES&T air, 2, 808-823, 10.1021/acsestair.4c00291, 2025.
Shilling, J. E., Zawadowicz, M. A., Liu, J., Zaveri, R. A., and Zelenyuk, A.: Photochemical Aging Alters Secondary Organic Aerosol Partitioning Behavior, ACS Earth and Space Chemistry, 3, 2704-2716, 10.1021/acsearthspacechem.9b00248, 2019.
Shiraiwa, M. and Pöschl, U.: Mass accommodation and gas–particle partitioning in secondary organic aerosols: dependence on diffusivity, volatility, particle-phase reactions, and penetration depth, Atmospheric Chemistry and Physics, 21, 1565-1580, 10.5194/acp-21-1565-2021, 2021.
Shiraiwa, M., Pfrang, C., Koop, T., and Pöschl, U.: Kinetic multi-layer model of gas-particle interactions in aerosols and clouds (KM-GAP): linking condensation, evaporation and chemical reactions of organics, oxidants and water, Atmospheric Chemistry and Physics, 12, 2777-2794, 10.5194/acp-12-2777-2012, 2012.
Song, K., Tang, R., Li, A., Wan, Z., Zhang, Y., Gong, Y., Lv, D., Lu, S., Tan, Y., Yan, S., Yan, S., Zhang, J., Fan, B., Chan, C. K., and Guo, S.: Particulate organic emissions from incense-burning smoke: Chemical compositions and emission characteristics, Science of The Total Environment, 897, 10.1016/j.scitotenv.2023.165319, 2023.
Song, K., Guo, S., Gong, Y. Z., Lv, D. Q., Zhang, Y., Wan, Z. C., Li, T. Y., Zhu, W. F., Wang, H., Yu, Y., Tan, R., Shen, R. Z., Lu, S. H., Li, S. D., Chen, Y. F., and Hu, M.: Impact of cooking style and oil on semi-volatile and intermediate volatility

organic compound emissions from Chinese domestic cooking, Atmospheric Chemistry and Physics, 22, 9827-9841, 10.5194/acp-22-9827-2022, 2022.
Sun, P., Liu, Y., Li, Y., Nie, W., Chi, X., Xu, Z., Zhong, S., and Yu, J.: Unified Source Apportionment of Organic Aerosols and Volatile Organic Compounds Reveals Underestimated Cooking Impacts in Urban Air Quality, Am. Chem. Soc. Environ. Sci. Technol. Air., 3, 73-82, 10.1021/acsestair.5c00210, 2026.
Takhar, M., Li, Y., and Chan, A. W. H.: Characterization of secondary organic aerosol from heated-cooking-oil emissions: evolution in composition and volatility, Atmospheric Chemistry and Physics, 21, 5137-5149, 10.5194/acp-21-5137-2021, 2021.
Takhar, M., Stroud, C. A., and Chan, A. W. H.: Volatility Distribution and Evaporation Rates of Organic Aerosol from Cooking Oils and their Evolution upon Heterogeneous Oxidation, ACS Earth and Space Chemistry, 3, 1717-1728, 10.1021/acsearthspacechem.9b00110, 2019.
Takhar, M., Li, Y., Ditto, J. C., and Chan, A. W. H.: Formation pathways of aldehydes from heated cooking oils, Environ Sci Process Impacts, 10.1039/d1em00532d, 2022.
Tan, R., Guo, S., Lu, S., Wang, H., Zhu, W., Yu, Y., Tang, R., Shen, R., Song, K., Lv, D., Zhang, W., Zhang, Z., Shuai, S., Li, S., Chen, Y., and Ding, Y.: Characteristics and Secondary Organic Aerosol Formation of Volatile Organic Compounds from Vehicle and Cooking Emissions, Atmosphere-Basel, 14, 10.3390/atmos14050806, 2023.
Tikkanen, I. P., Buchholz, A., Ylisirniö, A., Schobesberger, S., Virtanen, A., and Yli-Juuti, T.: Comparing secondary organic aerosol (SOA) volatility distributions derived from isothermal SOA particle evaporation data and FIGAERO-CIMS measurements, Atmospheric Chemistry and Physics, 20, 10441-10458, 10.5194/acp-20-10441-2020, 2020.
Wang, H., Guo, S., Yu, Y., Shen, R., Zhu, W., Tang, R., Tan, R., Liu, K., Song, K., Zhang, W., Zhang, Z., Shuai, S., Xu, H., Zheng, J., Chen, S., Li, S., Zeng, L., and Wu, Z.: Secondary aerosol formation from a Chinese gasoline vehicle: Impacts of fuel (E10, gasoline) and driving conditions (idling, cruising), Sci Total Environ, 795, 10.1016/j.scitotenv.2021.148809, 2021.
Wang, X., Chen, Y., Wang, F., Lu, Y., Huang, Z., Wang, W., Wang, Y., and Li, J.: Effects of ammonium sulfate on the hygroscopic properties and phase transition of aerosols with organic surrogates related to biomass burning and atmospheric oxidation, Atmospheric Research, 329, 10.1016/j.atmosres.2025.108464, 2026.
West, C. P., Hsu, Y.-J., MacFeely, K. T., Huston, S. M., Aridjis-Olivos, B. P., Morales, A. C., and Laskin, A.: Volatility Measurements of Individual Components in Organic Aerosol Mixtures Using Temperature-Programmed Desorption–Direct Analysis in Real Time–High Resolution Mass Spectrometry, Analytical Chemistry, 95, 7403-7408, 10.1021/acs.analchem.3c00923, 2023.
Xiao, L., Wang, S., Wang, Y., Wang, B., Ji, C., Lin, X., Liang, H., Zhang, S., Xu, X., and Dong, L.: Density functional theory studies on the oleic acid thermal oxidation into volatile compounds, Food Chem. X, 19, 10.1016/j.fochx.2023.100737, 2023.
Yang, Y., Yang, L., Zheng, M., Cao, D., and Liu, G.: Data acquisition methods for non-targeted screening in environmental analysis, TrAC Trends in Analytical Chemistry, 160, 10.1016/j.trac.2023.116966, 2023.
Yao, Y., Qiang, Z., Zhang, M., Lin, J., and Li, C.: Thermal oxidation mechanism of palmitic aicd, Food Research International, 186, 114372, https://doi.org/10.1016/j.foodres.2024.114372, 2024.
Ye, L., Zhang, F., Zhang, L., and Qi, F.: Theoretical studies on the unimolecular decomposition of propanediols and glycerol, Journal of Physical Chemistry A, 116, 4457-4465, 10.1021/jp301424k, 2012.
Ylisirniö, A., Barreira, L. M. F., Pullinen, I., Buchholz, A., Jayne, J., Krechmer, J. E., Worsnop, D. R., Virtanen, A., and Schobesberger, S.: On the calibration of FIGAERO-ToF-CIMS: importance and impact of calibrant delivery for the particle-phase calibration, Atmospheric Measurement Techniques, 14, 355-367, 10.5194/amt-14-355-2021, 2021.
Ylisirniö, A., Hyttinen, N., Li, Z., Alton, M. W., Nissinen, A., Pullinen, I., Miettinen, P., Yli-Juuti, T., and Schobesberger, S.: The saturation vapor pressures of higher-order polyethylene glycols and achieving a wide calibration range for volatility measurements by FIGAERO-CIMS, Atmospheric Measurement Techniques, 18, 6449-6464, 10.5194/amt-18-6449-2025, 2025.
Yu, Y., Guo, S., Wang, H., Shen, R. Z., Zhu, W. F., Tan, R., Song, K., Zhang, Z. R., Li, S. D., Chen, Y. F., and Hu, M.: Importance of Semivolatile/Intermediate-Volatility Organic Compounds to Secondary Organic Aerosol Formation from Chinese Domestic Cooking Emissions, Environ Sci Tech Let, 9, 507-512, 10.1021/acs.estlett.2c00207, 2022.
Zaveri, R. A., Shilling, J. E., Zelenyuk, A., Liu, J., Bell, D. M., D'Ambro, E. L., Gaston, C. J., Thornton, J. A., Laskin, A., Lin, P., Wilson, J., Easter, R. C., Wang, J., Bertram, A. K., Martin, S. T., Seinfeld, J. H., and Worsnop, D. R.: Growth Kinetics and Size Distribution Dynamics of Viscous Secondary Organic Aerosol, Environmental Science & Technology, 52, 1191-1199, 10.1021/acs.est.7b04623, 2018.

Zeng, J., Yu, Z., Mekic, M., Liu, J., Li, S., Loisel, G., Gao, W., Gandolfo, A., Zhou, Z., Wang, X., Herrmann, H., Gligorovski, S., and Li, X.: Evolution of Indoor Cooking Emissions Captured by Using Secondary Electrospray Ionization High-Resolution Mass Spectrometry, Environmental Science & Technology Letters, 7, 76-81, 10.1021/acs.estlett.0c00044, 2020.

Zhang, D., Cao, Y., Zhang, P., Liang, J., Xue, K., Xia, Y., and Qi, Z.: Investigation of the thermal decomposition mechanism of glycerol: The combination of a theoretical study based on the Minnesota functional and experimental support, Physical Chemistry Chemical Physics, 23, 20466-20477, 10.1039/d1cp01526e, 2021.

Zhang, H., Yee, L. D., Lee, B. H., Curtis, M. P., Worton, D. R., Isaacman-VanWertz, G., Offenberg, J. H., Lewandowski, M., Kleindienst, T. E., Beaver, M. R., Holder, A. L., Lonneman, W. A., Docherty, K. S., Jaoui, M., Pye, H. O. T., Hu, W., Day, D. A., Campuzano-Jost, P., Jimenez, J. L., Guo, H., Weber, R. J., de Gouw, J., Koss, A. R., Edgerton, E. S., Brune, W., Mohr, C., Lopez-Hilfiker, F. D., Lutz, A., Kreisberg, N. M., Spielman, S. R., Hering, S. V., Wilson, K. R., Thornton, J. A., and Goldstein, A. H.: Monoterpenes are the largest source of summertime organic aerosol in the southeastern United States, Proc Natl Acad Sci U S A, 115, 2038-2043, 10.1073/pnas.1717513115, 2018.

Zhang, J., Zuend, A., Top, J., Surdu, M., Haddad, I. E., Slowik, J. G., Prevot, A. S. H., and Bell, D. M.: Estimation of the Volatility and Apparent Activity Coefficient of Levoglucosan in Wood-Burning Organic Aerosols, Environmental Science & Technology Letters, 11, 1214-1219, 10.1021/acs.estlett.4c00608, 2024.

Zhang, X., Pandis, S. N., and Seinfeld, J. H.: Diffusion-Limited Versus Quasi-Equilibrium Aerosol Growth, Aerosol Science and Technology, 46, 874-885, 10.1080/02786826.2012.679344, 2012.

Zhang, Z., Zhu, W., Hu, M., Wang, H., Chen, Z., Shen, R., Yu, Y., Tan, R., and Guo, S.: Secondary Organic Aerosol from Typical Chinese Domestic Cooking Emissions, Environmental Science & Technology Letters, 8, 24-31, 10.1021/acs.estlett.0c00754, 2020.

Zhang, Z., Zhu, W., Hu, M., Wang, H., Tang, L., Hu, S., Shen, R., Yu, Y., Song, K., Tan, R., Chen, Z., Chen, S., Canonaco, F., Prévôt, A. S. H., and Guo, S.: Secondary organic aerosol formation in China from urban-lifestyle sources: Vehicle exhaust and cooking emission, Science of the Total Environment, 857, 10.1016/j.scitotenv.2022.159340, 2023.

Zhao, Y., Hu, M., Slanina, S., and Zhang, Y.: Chemical Compositions of Fine Particulate Organic Matter Emitted from Chinese Cooking, Environmental Science & Technology, 41, 99-105, 10.1021/es0614518, 2007.

Zhou, Z., Li, Y. L., Zhao, F., Xin, R., Huang, X. H., Zhang, Y. Y., Zhou, D., and Qin, L.: Unraveling the Thermal Oxidation Products and Peroxidation Mechanisms of Different Chemical Structures of Lipids: An Example of Molecules Containing Oleic Acid, J Agr Food Chem, 70, 16410-16423, 10.1021/acs.jafc.2c06221, 2022.

Zhu, W., Guo, S., Zhang, Z., Wang, H., Yu, Y., Chen, Z., Shen, R., Tan, R., Song, K., Liu, K., Tang, R., Liu, Y., Lou, S., Li, Y., Zhang, W., Zhang, Z., Shuai, S., Xu, H., Li, S., Chen, Y., Hu, M., Canonaco, F., and Prévôt, A. S. H.: Mass spectral characterization of secondary organic aerosol from urban cooking and vehicular sources, Atmos. Chem. Phys., 21, 15065-15079, 10.5194/acp-21-15065-2021, 2021.

Zuend, A. and Seinfeld, J. H.: Modeling the gas-particle partitioning of secondary organic aerosol: the importance of liquid-liquid phase separation, Atmos. Chem. Phys., 12, 3857-3882, 10.5194/acp-12-3857-2012, 2012.